MAGNETIC STRUCTURE OF LOIHI SEAMOUNT, AN ACTIVE HOTSPOT VOLCANO IN THE HAWAIIAN ISLAND CHAIN

A Thesis

by

AMY J. LAMARCHE

Submitted to the Office of Graduate Studies of
Texas A&M University
in partial fulfillment of the requirements for the degree of

MASTER OF SCIENCE

December 2003

Major Subject: Oceanography

MAGNETIC STRUCTURE OF LOIHI SEAMOUNT, AN ACTIVE HOTSPOT VOLCANO IN THE HAWAIIAN ISLAND CHAIN

A Thesis

by

AMY J. LAMARCHE

Submitted to Texas A&M University
in partial fulfillment of the requirements
for the degree of

MASTER OF SCIENCE

Approved as to style and content by:

William W. Sager (Chair of Committee)	Niall C. Slowey (Member)
Mark E. Everett (Member)	Thomas W. C. Hilde (Member)
Wilford Gardner (Head of Department)	

December 2003

Major Subject: Oceanography

ABSTRACT

Magnetic Structure of Loihi Seamount, an Active Hotspot Volcano in the Hawaiian Island Chain. (December 2003)

Amy J. Lamarche, B.S., Fitchburg State College

Chair of Advisory Committee: Dr. William W. Sager

The use of geophysical techniques to image the interiors of active volcanoes can provide a better understanding of their structure and plumbing. The need for such information is especially critical for undersea volcanoes, whose environment makes them difficult to investigate. Because undersea volcanoes are made up of highly magnetic basaltic rock, it is possible to use variations in the magnetic field to explore the internal structure of such edifices. This study combines magnetic survey data from 12 research cruises to make a magnetic anomaly map of volcanically active Loihi, located in the Hawaiian Island chain. NRM intensities and susceptibility measurements were measured from recovered rock samples and suggest that magnetic properties of Loihi are widely varied (NRM intensities range from 1-157 A/m and susceptibilities from 1.26×10^{-3} to 3.62×10^{-2} S.I.). The average NRM intensity is 26 A/m. The size and strength of magnetic source bodies were determined by using various modeling techniques. A strongly magnetized shield can explain most of the anomaly with a large nonmagnetic zone inside, beneath the summit. Prominent magnetic highs are located along Loihi's north and south rift zone dikes and modeling solutions suggest strongly magnetized source bodies in these areas as well as a thin, magnetic layer atop the nonmagnetic zone. The strong magnetic

anomalies found along the volcano's rift zones cannot be readily attributed to recent lava flows at the surface. Instead, the source bodies must continue several kilometers in depth to give reasonable magnetization values and are interpreted as dike intrusions. Nonmagnetic anomalies at the summit and south of the summit suggest the presence of a magma system. The model solution suggests Loihi is an inhomogeneously magnetized seamount with highly magnetic dike intrusions along the rift zones with a nonmagnetic body at its center overlain with a magnetic layer.

Dedicated to those who helped me choose the right road.

ACKNOWLEDGEMENTS

Many thanks to those who helped gather data used in this research, including Dr. Alexander Malahoff and Dr. Jonathan Smith of the University of Hawaii. Dr. Maurice Tivey of Woods Hole Oceanographic Institution helped a great deal with the RTP anomaly map and Fourier Inversion. I'd also like to thank Michael Garcia of the University of Hawaii for lending me Loihi rock samples which were very valuable to this study and Dr. Stuart Hall for allowing me run the samples in his paleomagnetic lab at the University of Houston. Funding was provided from the National Science Foundation project # OCE-9811326.

For their time and patience, I'd like to thank my committee chair, Dr. William Sager, and committee members: Dr. Niall Slowey, Dr. Thomas Hilde, and Dr. Mark Everett. Thanks to Debora Berti, Molly Bayer, Marilyn Yeager, and Sandy Drews for both moral and technical support. Your listening, suggesting, and friendship vastly improved the quality of time I've spent in Texas. I also appreciated the cooperative attitude, encouragement, and technical assistance from students and professors in geological oceanography as well as from students and professors in geology and geophysics.

I greatly appreciated the long distance support (including financial) and encouragement from my parents and the moral support from my sister. Thank you, Jenn, for your unconditional friendship that always gives me a solid surface to stand on.

TABLE OF CONTENTS

Page

LIST OF FIGURES

FIGURE Page

LIST OF TABLES

INTRODUCTION

Intra-plate and spreading ridge seamounts are built from igneous rocks of basaltic composition. These rocks form a variety of features (intrusions, flows, and rubble) and rock types (basalt, gabbro, and hyaloclastite) that cause physical properties to vary throughout the seamount. Large-scale inhomogeneities can be delineated by collecting magnetic field data and can be used to evaluate the subsurface geology of underwater volcanoes. Therefore, the overall magnetic field of the seamount becomes a property that can be used to investigate internal structure.

Loihi Seamount is the active expression of the Hawaiian hotspot (Clague and Dalrymple, 1989; Moore et al., 1982). The processes by which a seamount grows are vertical accretion of lava flows erupted on top of each other, filling of fractures and fissures by intrusions (principally rift zone dikes and magma chambers), and filling of low spaces on flanks by landslides. The subsurface geology, including magma plumbing, hydrothermally altered zones, and lithology of the volcano, creates areas of highly variable magnetizations (Gee et al., 1988; 1989). In this study, I combine magnetic survey data, model magnetic anomalies, and use the magnetic rock properties of rock samples to learn about the internal magnetic structure of Loihi Seamount.

This thesis follows the style and format of *Journal of Geophysical Research*.

Geological Setting

The Hawaiian-Emperor chain has a clear age progression from 81 Ma at the north end to currently active volcanism at the southeast end (Keller et al., 1995; Clague and Dalrymple, 1989). It is thought that the chain was formed as the Pacific plate moved over the existing hotspot creating a linear string of volcanoes recording the history of Pacific Plate motion relative to the hotspot. Meiji, located at the NW end, is probably the oldest seamount, however, it is not well-dated. South of Meiji is Detroit Seamount, which has been dated at about 81 Ma using the Ar^{40}/Ar^{39} radiometric technique (Keller et al., 1995). Ages of Hawaiian-Emperor Seamounts become progressively younger to the SE, ending at the Island of Hawaii and currently forming Loihi Seamount, which is thought to be sitting atop the Hawaiian hotspot (Clague and Dalrymple, 1989; Garcia et al., 1995).

Generally, island chain volcanoes have a well-defined life cycle. Initial eruptions are comprised of alkalic basalts (Moore et al., 1982). Shield building eruptions follow, consisting mostly of tholeiitic magma produced by higher degrees of partial melting when the volcano is centered over the hotspot (Frey and Clague, 1983). As activity of the submarine volcano declines, the lava reverts to an alkalic phase creating the "cap" of the seamount. After the main eruptive phases, a quiescent interval may occur lasting about 5-7 m.y. (Clague and Dalrymple, 1989) up to perhaps 18 m.y. (Lonsdale et al., 1993). Eruptions after the quiescent interval, sometimes termed "post erosional" may follow, usually low in volume and alkalic in nature.

Loihi is located at 18º54.28'N latitude and 155º15.28'W longitude, approximately 30 km southeast of the island of Hawaii (Fig. 1) and sits atop the flank of Kilauea Volcano. Its summit rises to about 980 m below sea level from a base 4700 m below sea-surface (Fig. 2). Loihi is in a youthful stage of growth (Klein, 1982; Clague and Dalrymple, 1989) with pronounced north-south rift zone ridges, which are thought to form early in Hawaiian Shield development (Fornari et. al., 1988). Pit craters also characterize Hawaiian shield volcanoes, especially when the volcano is in its shield building stage. There are 3 pit craters on Loihi's summit platform ranging from about 73-146 m in depth (Malahoff, 1987; Loihi Science Team, 1997).

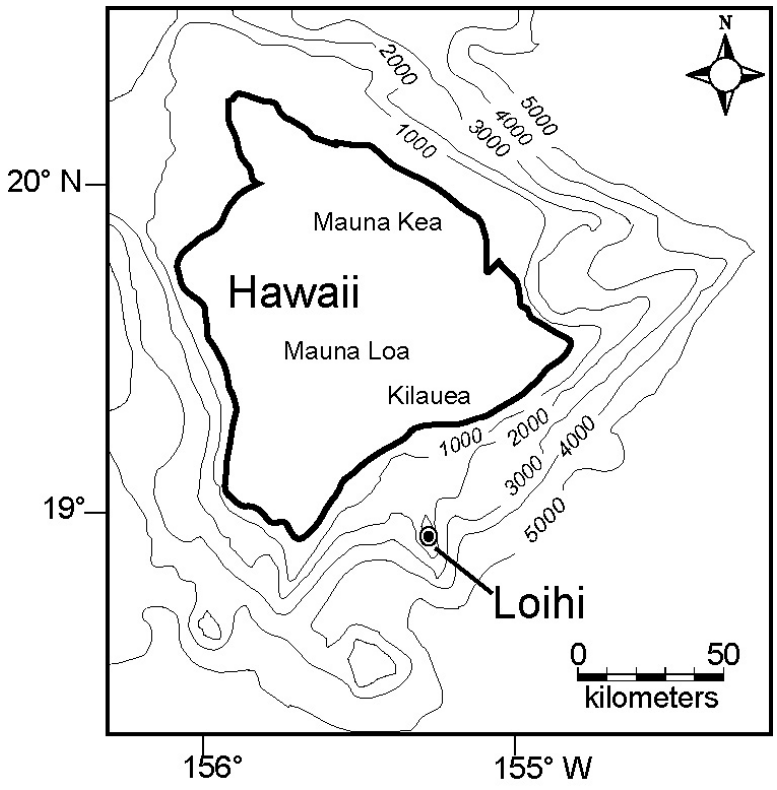

Figure 1. Location of Loihi Seamount.

Seismic events were monitored at Loihi in the late 1970's (Klein, 1982) with both shallow and deep focus earthquakes recorded. The deep earthquakes provide evidence that Loihi is not a vent of nearby Kilauea, but instead a separate volcano. Furthermore, the lavas of Kilauea and Loihi have been analyzed and it has been concluded that each volcano is chemically distinct and therefore erupt from separate sources (Staudigel et al., 1984). The last Loihi eruption was recorded in 1996 by the U.S. Geological Survey's Hawaiian Volcano Observatory (HVO) using its network of seismic detectors (Loihi Science Team, 1997). Between July 16 and August 9, 1996, more than 4000 earthquakes were detected making it the largest swarm of earthquakes ever observed at a Hawaiian volcano (Loihi Science Team, 1997).

Magnetic Inhomogeneities and Associated Volcanic Structures

Magnetic inhomogeneities in a volcano exist for various reasons. Lesser than average inhomogeneities may be the magnetic signature for heated basalts, hyaloclastites, and/or mass-wasting deposits. Initially, young basalts have relatively low Curie temperatures, above approximately 200°C they are nonmagnetic (Irving, 1970; Johnson and Atwater, 1978). Active volcanic structures (e.g., magma chambers and active rift zone ridges) tend to be above the low Curie point and therefore produce a nonmagnetic anomaly (Malahoff, 1987; Hildenbrand et. al., 1993). Hyaloclastites are basalts that have been extensively altered through interaction with seawater (Bonatti, 1967) and low temperature hydrothermal alteration, which degrades the magnetic minerals (Bonatti, 1967; Gee et al., 1993; Tivey and Johnson, 1990; Hildenbrand et al., 1993).

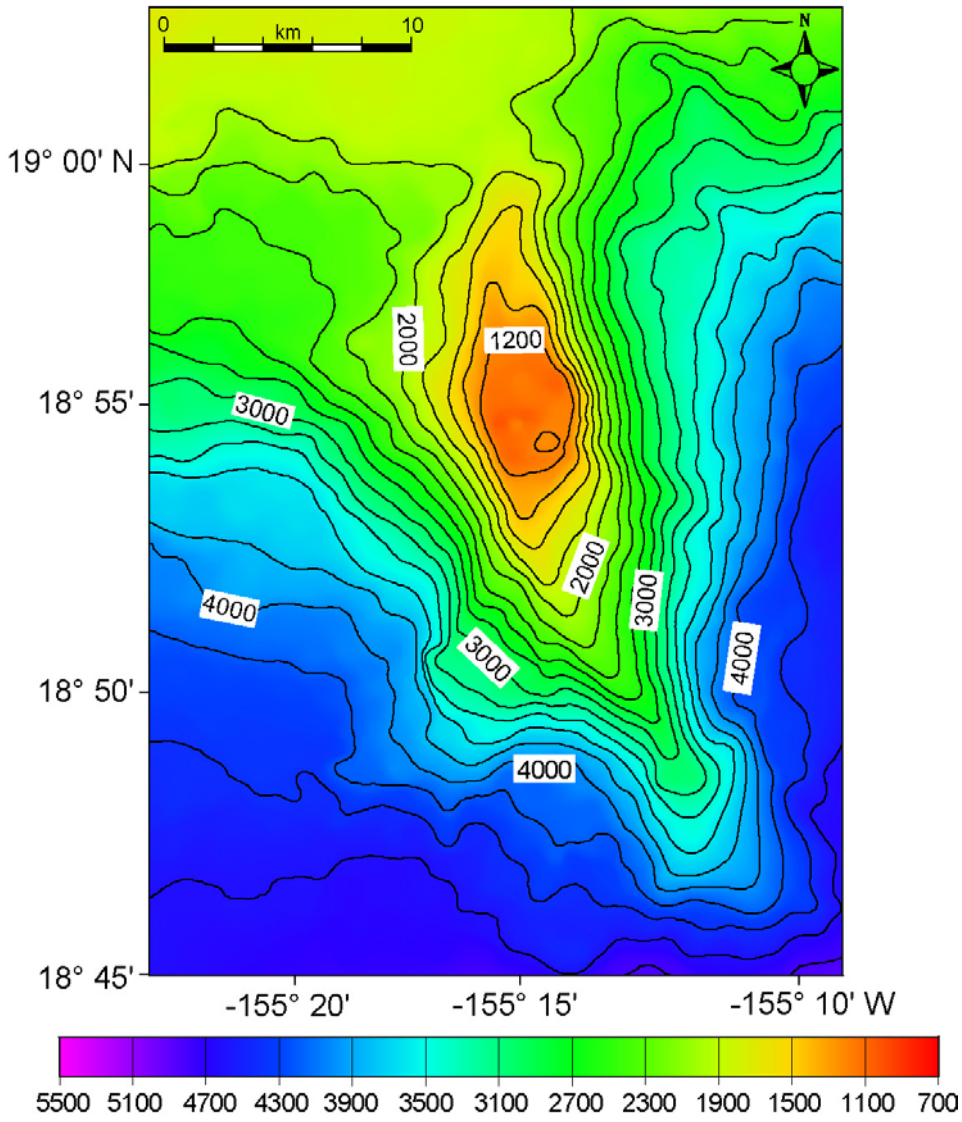

Figure 2. Multibeam bathymetry map of Loihi Seamount. Data was provided by the University of Hawaii. Contour interval is 200-m.

Mass-wasting deposits have been found to be a primary process during the growth of oceanic shield volcanoes (Holcomb and Searle, 1991; Moore et al., 1994; Lenat et al., 2001) and debris is commonly incorporated in submarine flanks. Debris

material consists of many rotated fragments with magnetic directions that cancel each other and thereby being incoherent expressed as a low magnetic anomaly.

Greater than average inhomogeneities are related to age, cooling history, and possibly whole rock chemistry of the material. Freshly erupted basalts are strongly magnetic (Hildenbrand, 1993; Tivey, 1994) because they have not been exposed at length to demagnetization processes. Cooling history also seems to have a definite affect on magnetic intensity. A rapid cooling rate produces fine-grained titanomagnetite which generally has a high NRM. High magnetization may be correlated with whole rock chemistry. For example, in a study of the magnetic properties from Loihi Seamount a strong positive correlation was recorded between NRM and TiO_2 (Johnson and Clague, 1981). However, a study of highly magnetic samples from a new submarine lava flow from the Juan de Fuca ridge found little correlation between FeO* and NRM (Johnson and Tivey, 1995).

Both greater and lesser than average inhomogeneities have been used to identify primary volcanic structures in active and dormant volcanoes by modeling magnetic survey data. Magnetic modeling of dormant volcanoes has detected the presence of several structures. The presence of hyaloclastites, creating a nonmagnetic seamount summit, effectively improved the fit of several dormant seamount models (Harrison, 1971). Other dormant terrestrial volcanoes including those in the Hawaiian Chain, Reunion Island, and Gran Canaria in the Canary Island Chain were found to have highly magnetic intrusive volcanic plugs in their center (Malahoff and Woolard, 1966; Lenat et al., 1987; Blanco-Montenegro et al., 2003). Anomaly highs were also seen over rift zone

ridges including volcanoes in the Hawaiian Chain (Malahoff and Woolard, 1966). More specifically, a broad study investigating the magnetic field of Kilauea confirmed an intense anomaly high over the major feature of the volcano, the east rift zone ridge (Lenat, 1987).

Active volcanoes have shown both low and nonmagnetic anomalies with magma chambers, central vent areas, and active rift zone ridges. Axial Seamount was found to have a summit negative anomaly thought to be caused by the presence of a magma chamber (Tivey and Johnson, 1990). The hot rock present in the magma chamber is probably the same source located in central vent areas and fissures producing large negative anomalies over the Hawaiian Ridge (Malahoff and Woolard, 1966). Active Kilauea Volcano has been studied several times. Similar to Axial Seamount, the center of Kilauea produces a magnetic anomaly low (Malahoff and Woolard, 1968) locating the magma chamber which is both hot and shallow (Furumoto, 1978). Kilauea's eastern dike complex also produced a low magnetic anomaly where inside temperatures were estimated to be over 1000ºC (Furumoto, 1978).

The magnetic structure of Loihi's Summit was investigated by Malahoff (1987) using a 2-dimensional modeling technique. A bulk magnetization of 75 A/m was used for the main volcano, which falls between values for dredge samples of 20-130 A/m reported in an abstract by Johnson and Clague (1981). Malahoff described 3 levels of anomaly. He described a long wavelength anomaly, approximately 20 km long, with normal polarity and an amplitude of 3500 nT, with a shorter 8 km long wavelength, reversed polarity anomaly with an amplitude of 1600 nT imbedded within the larger. An

even shorter wavelength, 300 m long, normal polarity anomaly with an amplitude of 200 nT was found within the reversed anomaly. Because Loihi has formed during the Brunhes Normal Polarity chron, it is unlikely that it contains a significant reversed polarity magnetization. Therefore, Malahoff interpreted the reversed anomaly as a nonmagnetic block at the summit, approximately 7 km wide and 3 km deep, likely to be a magma chamber and heated rock. The smaller, normal polarity anomaly within the nonmagnetic block was explained as a highly magnetic column about 1 km in width dividing the nonmagnetic block in half.

Anomaly Field and Modeling Methods

The distribution of magnetization within seamounts can be investigated by several methods. The shape of the anomaly depends on the shape of the seamount, direction of magnetization, and latitude of location. At a latitude other than 0º or 90º the observed anomaly appears offset from its sources and asymmetric with any given source producing both high and low anomalies (Fig. 3). The anomaly will appear positive where the seamount field has a component parallel to geomagnetic field and negative where it has a component in the opposite direction. The reduced-to-poles transformation (RTP) method (Bhattacharyya, 1965) is used to significantly reduce asymmetry and shift anomalies over their sources.

Forward models are used for investigation of more complicated magnetization distributions (Talwani, 1965; Plouff, 1976). Through trial and error, inhomogeneties in magnetization can be used to model the complex features of the magnetic anomaly. Inversions use simplified assumptions about the seamount magnetization, typically

assuming the existence of a homogenous magnetization (Richards et al., 1967) or a homogeneous magnetization with random homogeneities distributed throughout the seamount (Parker et al., 1987). In order to reveal the size and strength of the homogenous magnetization, least squares inversion of magnetic fields can be made (Richards et al., 1967; McNutt, 1986; Sager and Pringle, 1987).

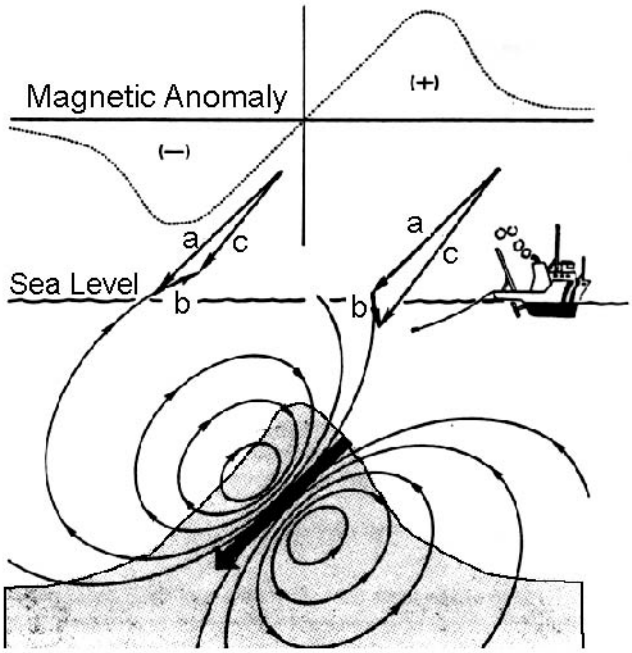

a-Magnetic Field Vector
b-Magnetic Anomaly Vector
c-Total Field Vector

Figure 3. Schematic of a seamount magnetic anomaly. Shaded area is cross section of a seamount and the large arrow is its mean magnetization vector. The sum of the seamount and ambient geomagnetic field produces the observed anomaly. If the direction of the seamount field (b) has a component opposing the main field (a), then the resultant vector (c) is smaller and a negative anomaly results (left). If the seamount field adds to the main field, a positive anomaly results (right). The shape of the anomaly depends on the shape of the seamount and the direction of the mean magnetization vector [Sager, 1992].

Rock Magnetic Properties

A seamount's magnetic field comes from the combination of remanent and induced magnetization. Thus, natural remanent magnetization intensity (NRM) and susceptibility (χ) are the most pertinent properties that can be used for constraining anomaly models. NRM is the bulk remanent magnetization of a rock and is dependent on geomagnetic field and geological processes during the history of the rock. Two primary components affecting the NRM of a rock are thermoremanent magnetization (TRM), which is acquired during cooling, and chemical remanent magnetization (CRM) formed by growth of ferromagnetic grains below the Curie temperature. Susceptibility is the ratio of the magnetization in a rock (J_i) to the corresponding magnetizing force (H). Rapidly cooled rocks will have a relatively high susceptibility and an even higher remanent magnetization mostly contributed from TRM. Low temperature submarine alteration often weakens the magnetization, sometimes reducing the magnetizations to zero (Watkins and Paster, 1971). Fresh basalts tend to have high NRM values of 0.06-100 A/m (Tivey and Johnson, 1990; Johnson et al., 1996) which decay exponentially as described by NRM = 25 $e^{-9.4t}$, where t is time in millions of years, and NRM is in A/m (Johnson and Tivey, 1995).

A problem that arises in some seamount modeling techniques is the assumption of an absent induced or viscous component. The magnetization a rock may acquire when exposed to a magnetic field is the induced magnetization (J_i) related to the susceptibility and the Earth's magnetic field by $J_i = \chi H$. The induced magnetization points in the direction of the present field whereas the remanent magnetization points in

the direction of the field during the eruption of seamount lavas. The Koenigsberger ratio (Q ratio) is the ratio of remanent to induced magnetization (J_r/J_i). Frequently, seamount basalts have Q values >10, which indicates the effect of the induced magnetization is negligible upon the overall direction. However, studies of rocks from large seamounts show that the induced magnetization may be 25 – 30% of the remanent magnetization (Gee et al., 1988, 1989).

METHODS

Cruise Data

Total magnetic field data were collected during 12 separate research cruises with proton magnetometers towed behind a ship. The primary survey data are from the R/V *Marskoye Geofisik,* a Russian research vessel that surveyed the south flank of Hawaii in 1991. This survey covers the entire study area, however, the ship tracks are widely spaced, approximately 3.5 km on the main steep part of the flanks and 7 km in remaining areas. To improve sampling density, other cruise data were used to fill in the gaps. The data were collected over a span of 20 years using a variety of navigational equipment (Table 1).

The differences in navigational equipment are important in determining navigational accuracy. Older technology, such as Doppler satellite navigation had inherent limitations of accuracy (~1/4 mile), long periods of time between updating the position of satellites (often many hours), and the usage of low-frequency measurements that caused sensitivity to small movements of the receiver as well as atmospheric noise (i.e. lightning) (Stewart and Joy, 1974). LORAN (Long RAnge Navigation), a radio triangulation method, also used low-frequency signals however, long-range accuracy was improved with a worldwide radio-navigation system. The system still had limited coverage (the receiver needed to be within 600-100 miles of a source) and the accuracy was dependent on atmospheric, electrical noise as well as source/receiver geometry (Takagi et al., 1980). GPS (Global Positioning System) technology increases accuracy by using a triangulation method utilizing satellites that emit a complex digital signal to

determine the position of reference points within a matter of meters. There are a large number of satellites so position fixes are nearly continuous (every 1 sec.). Delays the signal experiences due to atmospheric noise can be corrected because both time and distance are measured which increases its accuracy dramatically in comparison to past navigational technology.

Table 1. Surveys and navigation used to create magnetic anomaly map of Loihi Seamount.

Survey	Ship	Institution	Navigation
Haw761000	R/V Kana Keoki	Univ. of Hawaii	Doppler
Haw770926	R/V Kana Keoki	Univ. of Hawaii	Doppler
Haw7722000	R/V Kana Keoki	Univ. of Hawaii	Doppler
Haw801002	R/V Kana Keoki	Univ. of Hawaii	Doppler
Haw7781500	R/V Kana Keoki	Univ. of Hawaii	Doppler
MW8611	R/V Moana Wave	Univ. of Hawaii	GPS
USGS1978	R/V Lee	US Geol. Survey	LORAN
USGSf288	M/V Farnella	US Geol. Survey	LORAN, GPS
USGSf586	M/V Farnella	US Geol. Survey	LORAN, GPS
USGSf686	M/V Farnella	US Geol. Survey	LORAN, GPS
Atlant286	R/V Atlantis II	WHOI	GPS
	R/V Marskoye Geofisik	Acad. of Science	GPS

Layback Correction

The difference in position between the ship and the magnetometer is not recorded within the digital cruise data. The ships in these surveys are approximately 55-75 m in length and the usual layback is 3 ship-lengths or 165-225 m. All ship navigation was corrected for the offset with an estimated layback of 200 m.

Diurnal Correction

In order to correct for variations caused by external field activity, fluctuations in geomagnetic intensity during the surveys were recorded at a stationary observatory and subtracted from the total magnetic field data recorded by the towed magnetometer. These data were obtained from the NOAA magnetic observatory in Honolulu.

DGRF Correction

The Definitive Geomagnetic Reference Field (DGRF) was removed from the total magnetic field data to give magnetic anomaly values. The DGRF is a compilation of International Geomagnetic Reference Fields (IGRF). IGRF is the internationally accepted model of the direction and magnitude of the Earth's magnetic field and is updated every 5 years to account for secular variation (Jensen and Cain, 1962). The DGRF was appropriate for 1965 – 1995.

XOVER

XOVER (Wessel, 1989) is a program that evaluates offsets in data values where ship tracks cross. Detected offsets in data values at track crossings are called cross-over errors (COE's). Where a ship track crosses itself, the COE is termed "internal", whereas two tracks crossing from separate cruises give an "external" COE. The internal

comparison is useful because it checks the consistency of the ship's navigation within a single survey. External COE's show agreement between two different surveys. Primary causes of COEs in magnetic surveys are poor navigational accuracy in some cruises, especially older ones, as well as magnetic field fluctuations.

This study used the XOVER program to compare bathymetry and magnetics of the cruises listed in Table 1. The R/V *Marskoye Geofisik* data were used as reference navigation because of its wide coverage and GPS navigation. Remaining GPS navigated cruise data were then fit to the reference navigation and non-GPS cruise data added last. Position corrections in non-GPS cruise data were made by making small shifts (no more than 1-2 km) east, west, north, and/or south to the ship tracks in order to improve the match with better navigated tracks. COE's ranged from 0.6 – 410 nT and averaged 82 nT. In some instances, bathymetry data COE's were small, but magnetic data COE's were large. The match in bathymetry data indicates reliable navigation while the mismatch is magnetic data suggests an external influence, such as a solar storm, during one of the surveys. Segments of ship tracks with consistently high COE's (> 100 nT) were expunged from the data set.

Magnetic Anomaly Map

Corrected magnetic data were gridded using a bicubic spline technique in a GMT (Generic Mapping Tools; Wessel and Smith, 1991) program called surface.grd. Grid spacing is selected based on the spatial distribution of data points. Because our data set was irregularly spaced, the selected grid spacing was a compromise that tried to be not too large in order that well sampled anomaly features would be represented and not so

small that too many points were interpolated between actual data points. For the Loihi anomaly map, a grid spacing of 556 m was able to be used. The gridded data was then contoured at 100 nT intervals.

An RTP transformation (Bhattacharyya, 1965) was performed on the gridded anomaly. This transformation shifted the anomalies over their sources making it easier to determine where to place anomalous bodies using the directions of both the Earth's magnetic field and the total magnetization. The Geocentric Axial Dipole (GAD) averages the magnetic field from 10^4 -10^5 years and was used to account for the secular variation that is likely to have occurred during Loihi's growth. Because anomaly areas are easier to locate, the RTP transformation was used in the least squares and forward models.

Modeling

A Fourier magnetization inversion (Parker and Huestis, 1974) was used as a starting point in modeling the seamount magnetization because it is computer controlled and therefore "unbiased". The inversion uses the bathymetry of the seamount to define the upper surface of the source layer, assumes a constant source layer thickness, and inverts the magnetic field to find the magnetization distribution. For this model, wavelengths longer than 3 km were analyzed. A 3 km cutoff was chosen because wavelengths shorter than this appeared to oscillate because of the lack of data points over small wavelength features. For the final magnetization solution, an arbitrary number called the annihilator function is used. The amount of annihilator is chosen in order to balance the positive and negative magnetization values so that both

magnetizations will be equally represented in the model, even though in the case of Loihi, negative magnetization is unlikely. It is important to note that the choice of annihilator does not change the shape of the magnetization, only the positive and negative values. There are 3 important assumptions to note using the Fourier inversion. The first is that the source layer has a constant thickness. That is, the inversion uses the topography of the seamount and assumes the bottom of the seamount mirrors the surface so that a constant thickness is maintained. Next, the direction of the magnetization is allowed to vary in a horizontal plane, but not vertically. Lastly, the inversion allows both positive and negative magnetizations whether or not the sources contain polarity reversals.

Two other magnetization modeling techniques were used, one an inversion and the other a forward model. Both use algorithms to calculate the magnetic anomaly from a seamount with uniform magnetization by approximating depth contours as horizontal polygonal prisms over which volume integrals are performed (Plouff, 1976). Polygons were constructed following the multibeam bathymetry map (see Fig. 2). Each polygon is 200 m thick and has vertical sides (Fig. 4). Although the true shape of Loihi's bottom is unknown, the bottom of the polygonal approximation is sloped to account for its location on the sloping flank of Kilauea. The slope is expressed by the abrupt cutoff at the north end of each polygon below the 2400 m contour.

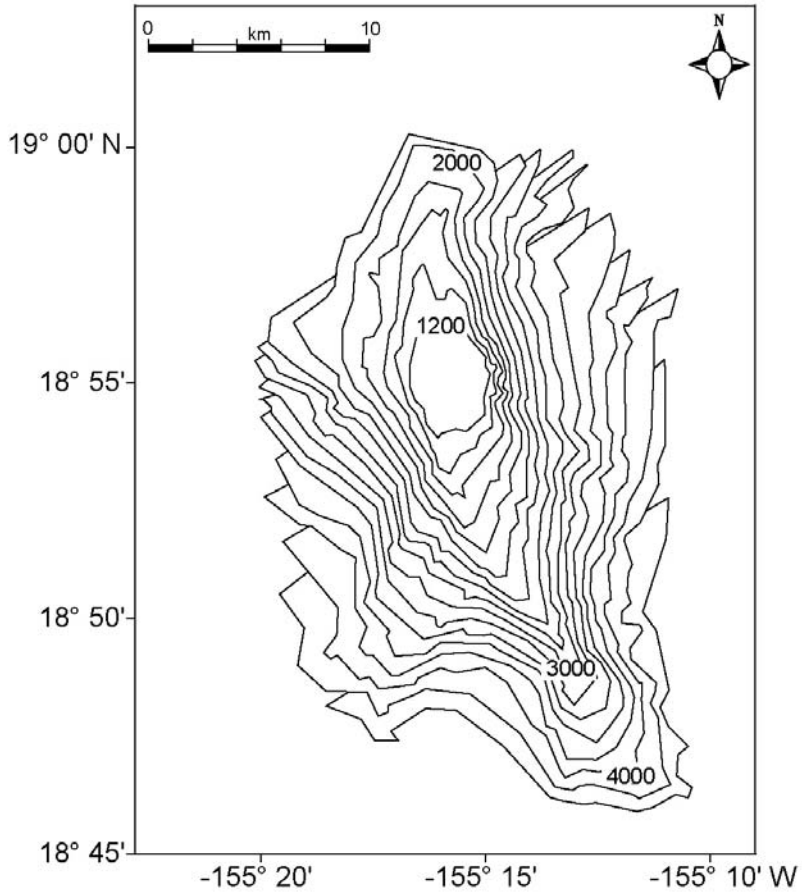

Figure 4. Polygon approximation of Loihi Seamount. Each polygon was estimated from multibeam bathymetry data at 200 m contours.

The inversion approach calculates the uniform magnetization that fits the observed anomaly closest in a least squares sense. In this inversion rendition, a calculated magnetic field of a uniformly magnetized body of arbitrary shape can be represented by a linear combination of the magnetization vector with the volume integral of the body (Plouff, 1976). Given the observed magnetic field and assuming the blocks are uniformly magnetized, two types of least squares inversions were used. The first allows the magnetization to have any average intensity, inclination, and declination to

minimize the residuals between observed and calculated anomalies. The second type of inversion was used in conjunction with forward modeling. This inversion uses fixed magnetization directions, set at the present field direction for the purpose of our study, and the amplitude is allowed to change. The combination of the inverse and forward modeling approach used in this study is best described as $B_{obs} = a + \Sigma_n m_i * B_{i,}$ where B_{obs} is the scalar observed magnetic field, a is the amount of constant offset between the observed and calculated anomaly, n is the number of source bodies within the inversion model, m_i is the magnetization amplitude of each body, and B_i is the unit magnetic field also produced by the forward model. The way this method was used was to make approximations of anomalous source body problems, calculate a unit magnetic field, and run the inversion to determine the best magnetization amplitudes, $B_{i,}$ for the anomalous bodies. Anomalous magnetic source bodies were constructed using residual anomalies from previously run models as a guide. Next, forward models were run for each body to produce the magnetization amplitude as well as the unit magnetic field. The inversion program accepted 1-5 source bodies and therefore some source bodies located near each other were grouped. Together, these quantities together were run as an inversion, which calculated the offset for each model.

Quality Indicators

I used 2 indicators to quantify how closely the computed anomaly fits the observed values. The first is the goodness-of-fit ratio (GFR). The GFR is the ratio of the mean observed anomaly field to the mean magnitude of the residual field. Using the GFR expression, a high number indicates a good "fit". Values less than 2 are usually

considered unreliable in seamount magnetic anomaly inversions (Sager, 1984). The GFR has been used on many seamount anomaly inversions and allows comparison of previous results. The least squares modeling technique uses a linear regression to make its calculations making it appropriate to measure the root mean square (RMS) misfit. The RMS misfit is the sum of the squared residuals defined as $[\sqrt{1/n_i \sum n(y_i - y_i')^2}]$ where n is the number of points, y_i is the observed field, and y_i' is the calculated field. The RMS misfit is essentially the average error.

Although there are statistical methods to compare differences between the calculated model to the observed (i.e. GFR and RMS misfit), they were not always the primary factor for rejecting or accepting a model. In some of the results, an increased GFR and a lower RMS misfit were obtained however factors such as unrealistic magnetizations, differences in shape of the produced wavelengths, and reduced residuals in a small area of the seamount were reasons to abandon, modify, or accept a model.

Rock Magnetic Properties

To compliment the modeling solutions, I measured magnetic properties of rock samples from Loihi collected using a submersible by Michael Garcia of the University of Hawaii. The rock samples have well-determined navigation and were located in and near the summit area (Fig. 5). The Alvin submersible was used to collect 13 samples in 1993. Ten samples were collected aboard the Pieces V submarine in 1990 and 15 during 1995. The NRM and susceptibility were measured. The size of samples 1804-4 and 1804-5 were too small to measure the NRM intensity however susceptibility values were successfully acquired. All NRM intensities were measured on an Agico JR-5A spinner

magnetometer and the susceptibilities were measured on a Barrington MS-2 susceptibility meter. These data are shown in Table 1 and can be used to evaluate the validity of modeled magnetizations.

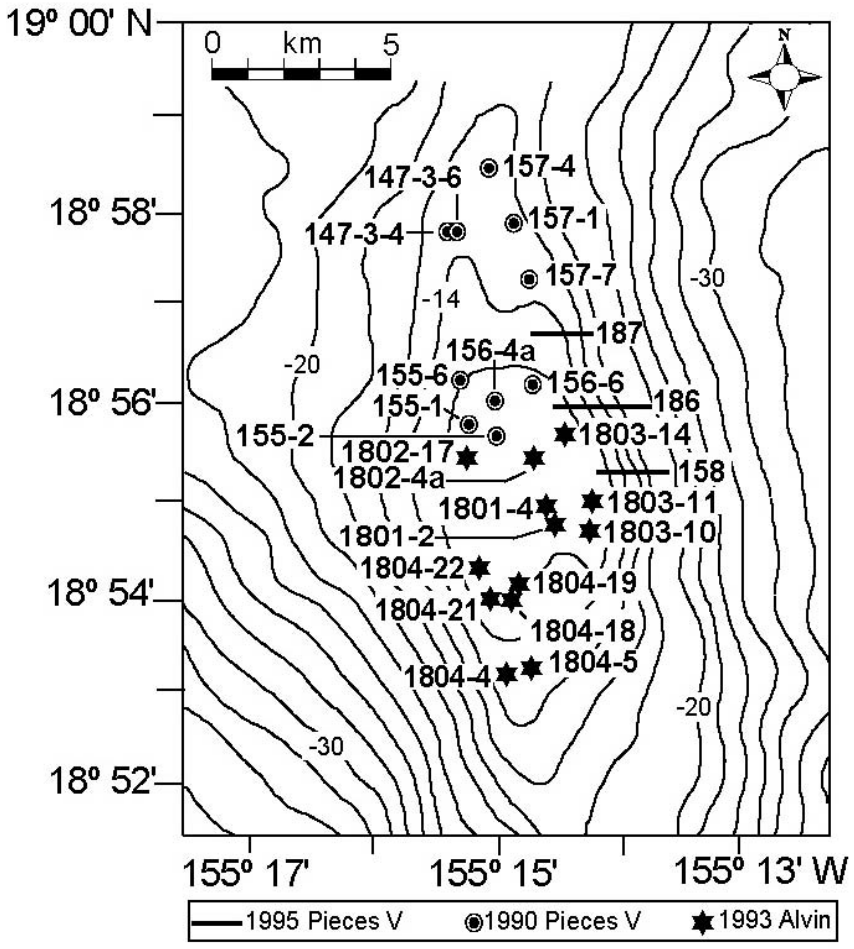

Figure 5. Locations of rock samples from which magnetic properties were measured.

RESULTS

Rock Magnetic Properties

The rock samples have NRM values ranging from 1 to 157 A/m and susceptibilities from 1.26 x 10^{-3} to 3.62 x 10^{-2} S.I. units (Table 2). Data indicate that the samples are strongly magnetized with a mean logarithmic intensity and susceptibility of 26 A/m and 5.0 x 10^{-3}, respectively. These values are higher than other recorded values of Hawaiian basalts as well as approximately an order of magnitude higher than oceanic ridge basalts. Calculated Q ratios average 191 which indicate that induced magnetization makes little contribution on the overall magnetization of the seamount.

Logarithmic histograms of NRM (Fig. 6) and susceptibility (Fig. 7) show normal distributions of both magnetic properties. The median value of NRM is 25 A/m and the susceptibility median is 5.0 x 10^{-3} S.I. Both values are close to their logarithmic averages. The graphs show that few high and low values exist and the majority of the measurements are close to both median values.

Attempts were made to observe patterns between NRM and susceptibility as well as spatial relationships that may exist. NRM values were plotted as a function of susceptibility (Fig. 8). A correlation coefficient of 0.29 suggests that there is no strong correlation between NRM and susceptibility. In contrast, a relationship between intensity and location is implied (Fig. 9). High values are present at the north and south rims of the summit platform. Mostly medium values exist over the central summit platform. Mixed values ranging from medium to high are over the north rift ridge. A larger range of intensities exist over transects up the east slope. The transects sample vertical flow succession and show values from low to high. If age dominates NRM intensity variation, low values would occur at lower depths and high values would occur at higher depths and the relationship would be easily seen along these transects. However, a relationship is not seen and the variable intensity suggests that flow NRM intensity is variable at a single location.

Table 2. Magnetic properties of samples from the summit region of Loihi Seamount.

Sample #	NRM (A/m)	X	J_i	Q
147 3-4	53.88	0.008	0.377	230.41
147 3-6	98.64	0.007	0.328	484.41
155-1	140.26	0.012	0.523	431.88
155-2	157.11	0.013	0.588	430.20
155-6	63.62	0.007	0.320	754.70
156-4a	121.90	0.020	0.905	216.82
156-6	63.62	0.008	0.345	296.89
157-1	90.02	0.008	0.342	424.25
157-4	23.45	0.009	0.399	94.72
157-7	15.64	0.003	0.130	194.26
158-1	24.29	0.004	0.189	206.94
158-3	78.04	0.036	1.628	77.18
158-4	50.84	0.007	0.330	248.15
158-7	3.05	0.015	0.679	7.23
186-1	14.75	0.006	0.251	94.53
186-2	11.54	0.007	0.305	60.83
186-3	9.78	0.012	0.544	28.96
186-5	19.24	0.007	0.299	127.05
186-8	2.68	0.014	0.646	138.43
186-9	28.72	0.006	0.261	103.76
186-10	13.66	0.013	0.599	6.67
186-11	22.02	0.006	0.279	177.15
186-14	110.27	0.029	1.283	36.69
187-2	15.93	0.029	1.294	19.81
187-5	3.97	0.001	0.060	106.79
1801-2	17.84	0.003	0.126	227.92
1801-4	46.62	0.005	0.220	341.36
1802-4a	5.58	0.001	0.057	325.33
1802-17	20.91	0.002	0.104	158.13
1803-10	31.75	0.005	0.247	206.91
1803-11	0.91	0.004	0.159	9.19
1803-14	8.70	0.021	0.966	14.49
1804-4	0.00	0.006	0.260	0
1804-5	0.00	0.012	0.546	0
1804-18	36.83	0.005	0.221	268.94
1804-19	43.57	0.012	0.551	127.43
1804-21	46.56	0.007	0.326	229.89
1804-22	71.01	0.007	0.296	385.93

NRM = natural remanent magnetization
X = susceptibility
J_i = induced magnetization
Q = Koenisberger ratio

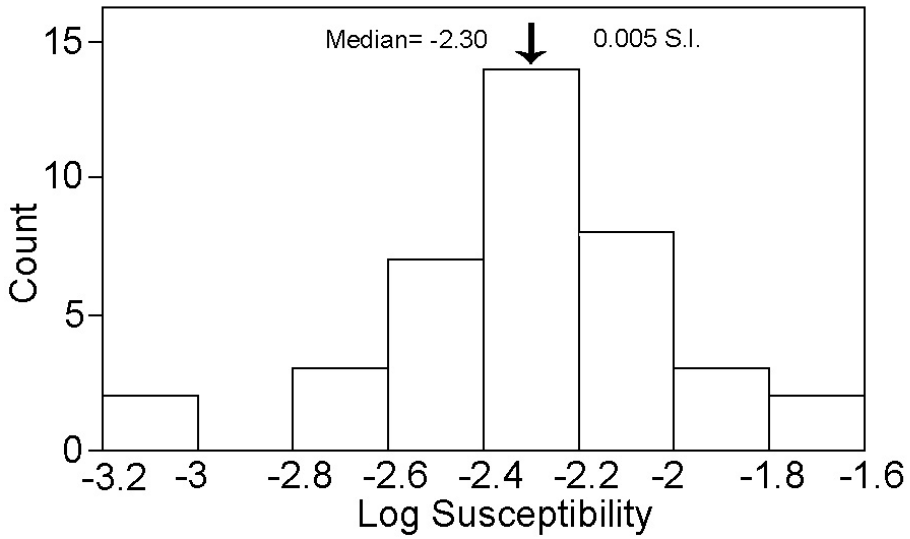

Figure 6. Histogram of logarithmic NRM for Loihi rock samples.

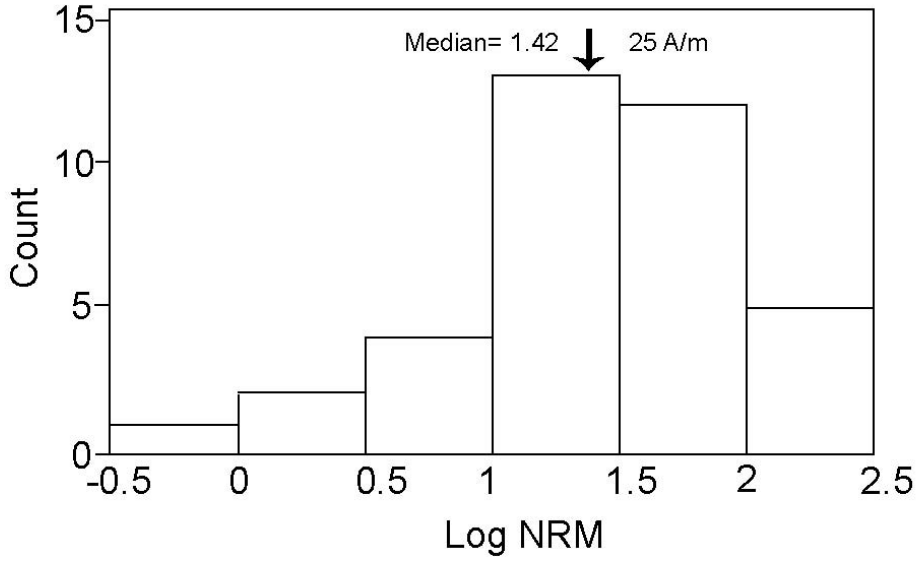

Figure 7. Histogram of logarithmic susceptibility for Loihi rock samples.

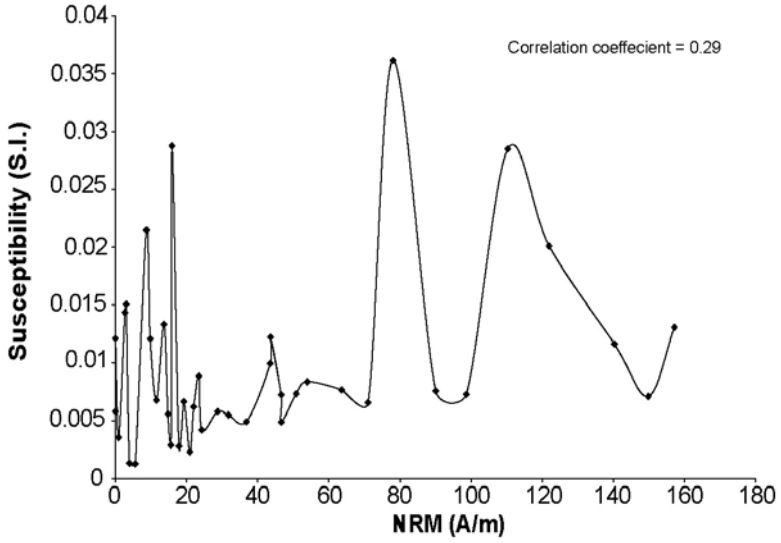

Figure 8. Susceptibility vs. NRM. A correlation coefficient of 0.29 suggests no significant relationship between the two axes.

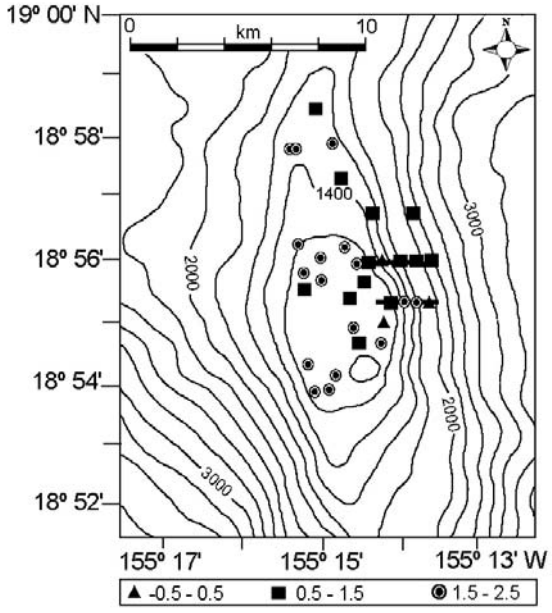

Figure 9. Spatial distribution of logarithmic NRM intensities plotted around the summit of Loihi. Bathymetry contours of 200 m are shown.

Loihi Magnetic Anomaly Map

The observed magnetic anomaly map is characterized by large amplitude magnetic lows and highs (Fig.10). Paired highs and lows are located on the north and south areas with the largest pair trending SE along the south rift ridge, and the smaller pair on the north side of the volcano. Magnetic lows occur over summit peaks, the eastern flank, and over the north rift ridge. The most negative anomaly values are on the tip of the north flank and extend west with values as low as –1600 nT. Just to the south of the anomalous low on the north rift ridge is a relative high anomaly. This anomaly trends SW-NE and peaks at 600 nT. The highest anomaly is located on the south rift zone ridge and reaches a value of 1800 nT slightly south of the summit platform. Altogether, the peak- to-trough amplitude of the magnetic anomaly is approximately 3200 nT.

The RTP transformation shifts the high anomalies over Loihi's rift zone ridges and the lows over the flanks. The high anomaly that covers the north rift ridge, branches slightly resembling an inverted "y", and continues down the south rift ridge. The anomaly then widens, bulging E-W slightly south of the anomaly peak. Over the north rift ridge, the lowest anomaly is pushed north. The peak of the positive anomaly becomes more elongated, and a magnetic low is apparent over the lower flanks. The RTP anomaly is at a minimum, i.e. a low saddle, over the summit platform (Fig.11).

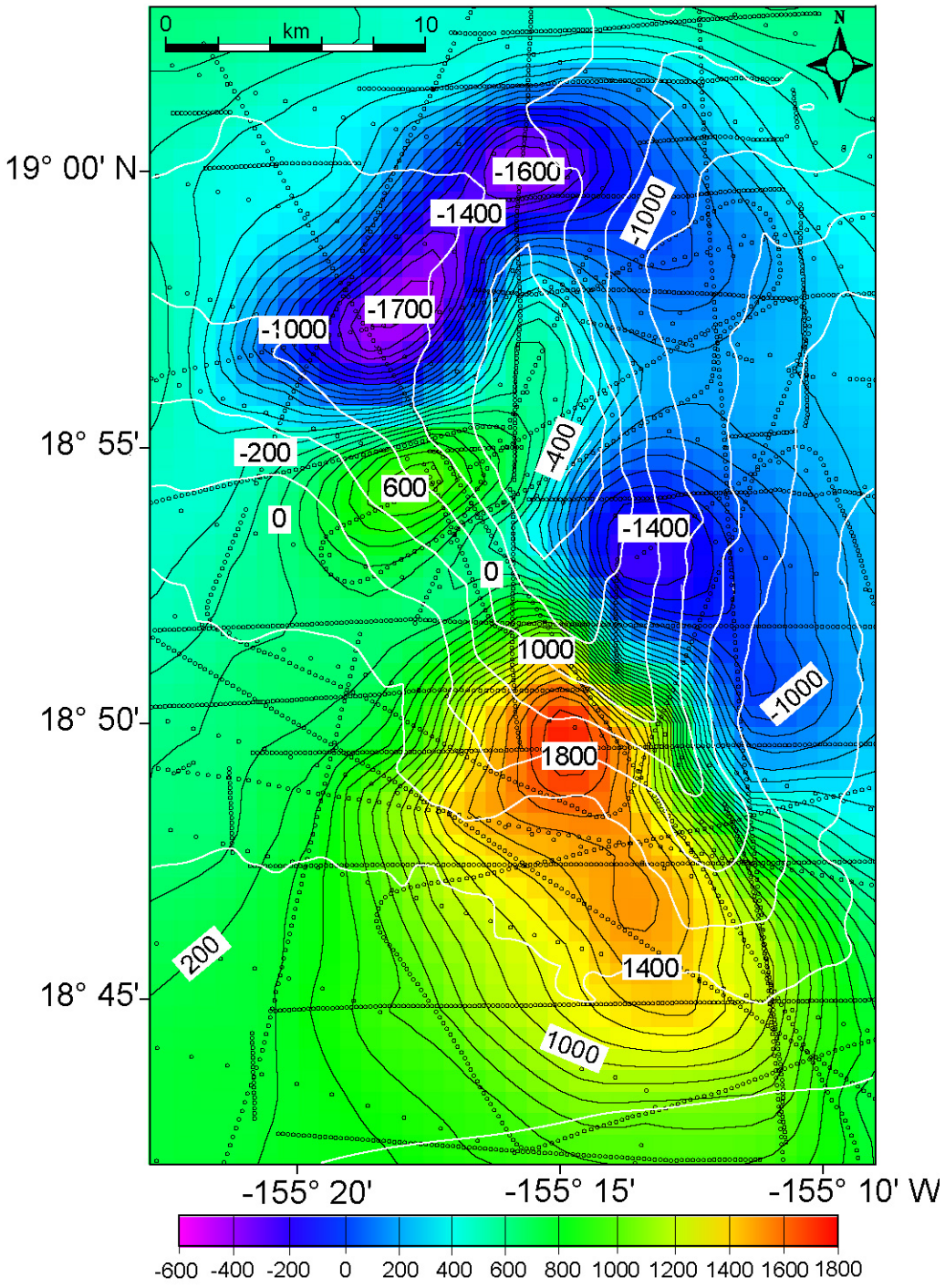

Figure 10. Observed total field magnetic anomaly map of Loihi. Contours are in 100 nT intervals. Open dots show the location of magnetic measurements along ship tracks and white contours show Loihi bathymetry at 500-m intervals for reference.

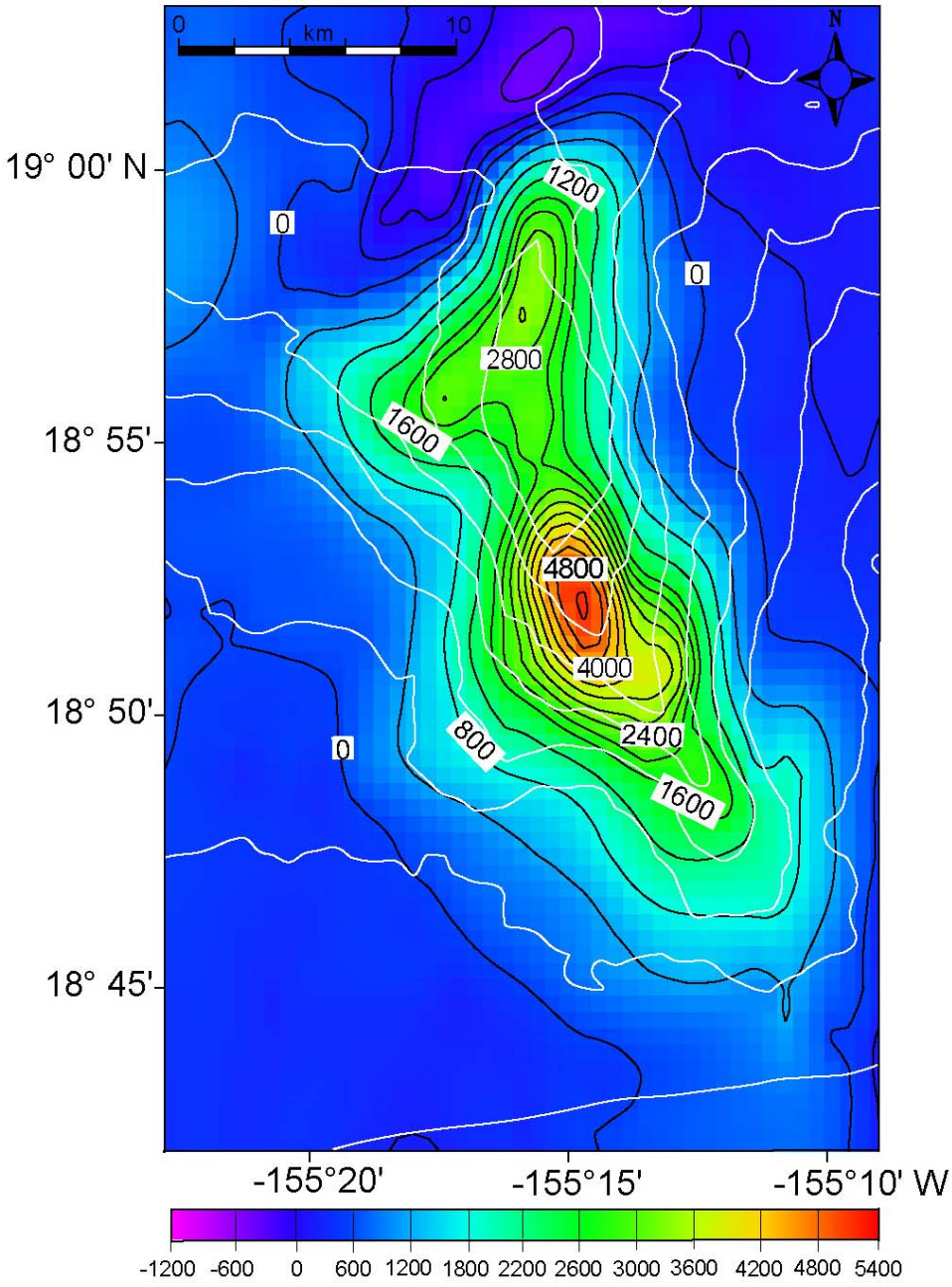

Figure 11. RTP transformation anomaly. Black contours depict the magnetic data and are contoured at 100 nT intervals. White contours show Loihi bathymetry for reference.

Magnetic Modeling of Loihi Seamount

Fourier Inversion

Similar anomalous features seen in the RTP magnetic anomaly maps exist in the Fourier inversion solution (Fig. 12), which is to be expected since the RTP shifts the positive anomalies above their sources. Anomalous highs vary from 10 – 20 A/m and are again present over the north and south rift zone ridges while low magnetization ranges from 0 - -25 A/m on the basal flanks. The biggest contrast between positive and negative anomalies exists on the SE flank where the difference is 45 A/m. This inversion provides more evidence for highly magnetic rift zone ridges with flanks of lower magnetization.

S1-Homogeneous Model

This model uses the polygonal approximation that follows the observed bathymetry known as shield model 1 (S1) and assumes that the bottom of the seamount is sloped and also that the magnetization is homogenous (Fig. 13). The solution produces high residuals (Fig. 14) and a calculated anomaly that is wider from east to west than the observed indicating that the flanks are less magnetic than predicted by the model (Fig. 15). High residual anomalies, a large RMS misfit of 1118 nT, and a GFR of only 1.17 (See Table 3) show that Loihi magnetization is not well fit by a homogenous model. The broad wavelength produced by seamount bathymetry is one factor that keeps the calculated magnetization low because of misfits on the flanks. The main factor, however, is the mismatch between the observed and the calculated anomalies is the difference in the location of the peaks. The observed anomaly peaks over the upper

south rift zone ridges (at 18˚52.5'N), but the calculated anomaly is highest over the summit.

S2-Homogenous Model

The bathymetry contours are re-digitized (S2) to follow the steeper upper slopes of the volcano (See Fig. 13). The idea is that the lesser slopes may be caused by talus, which would be expected to have an incoherent magnetization. Re-running the forward model using the modified layers results in residual anomalies that are less, but still high (Fig. 16). The GFR is almost the same at 1.39 and the RMS misfit increases to 974 nT. The S2 model produces a narrower wavelength almost matching the observed from west to east across the summit (Fig. 17). The fit from north to south, however, generates the vast majority of the error. However, because of the close fit seen in the EW profile, the S2 model is carried over into succeeding models.

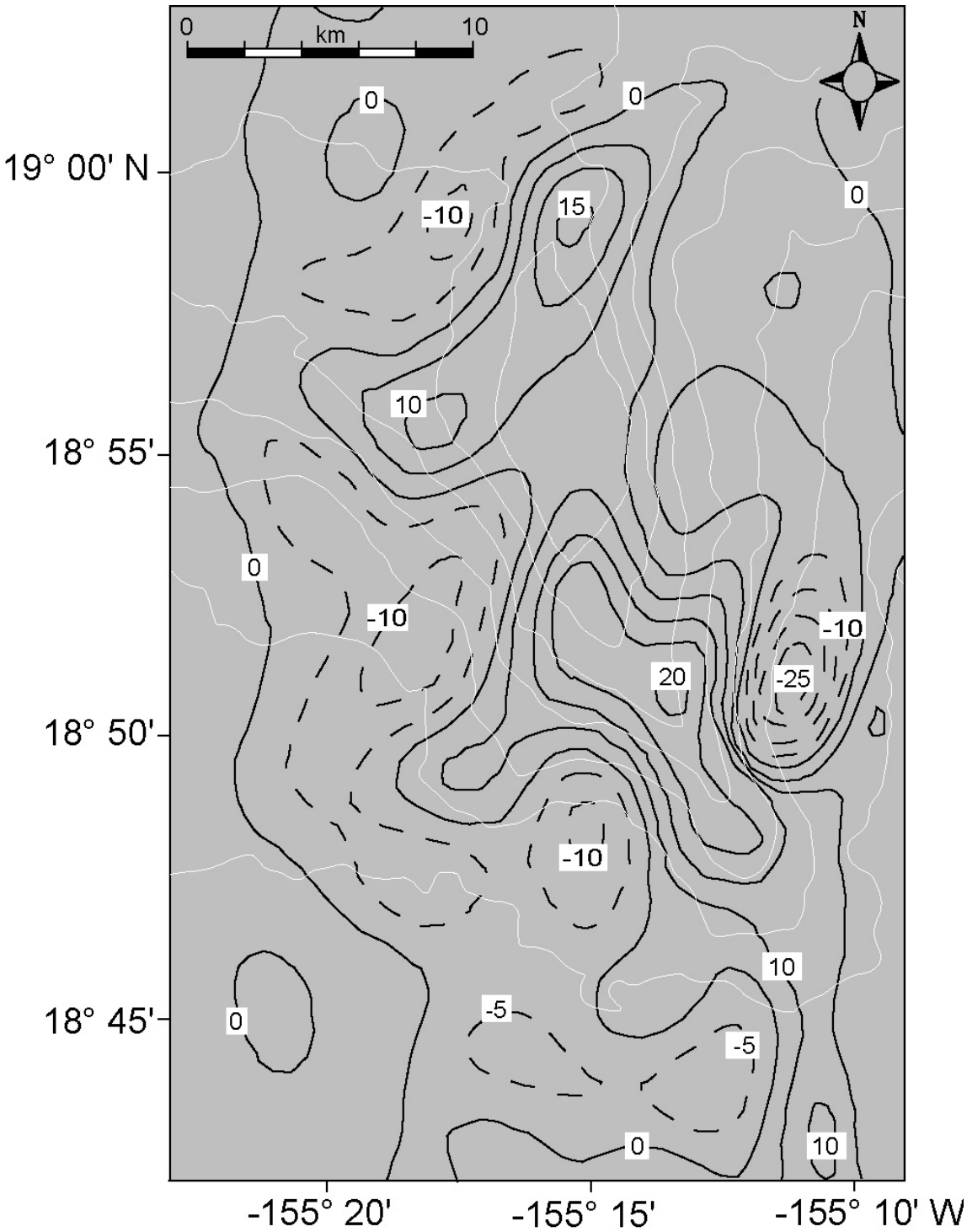

Figure 12. Fourier inversion solution using a 3 km wavelength cutoff. Black contours are the calculated magnetization solution at a 5 A/m contour interval. Solid lines are positive values and dotted are negative. White contours show Loihi bathymetry for reference.

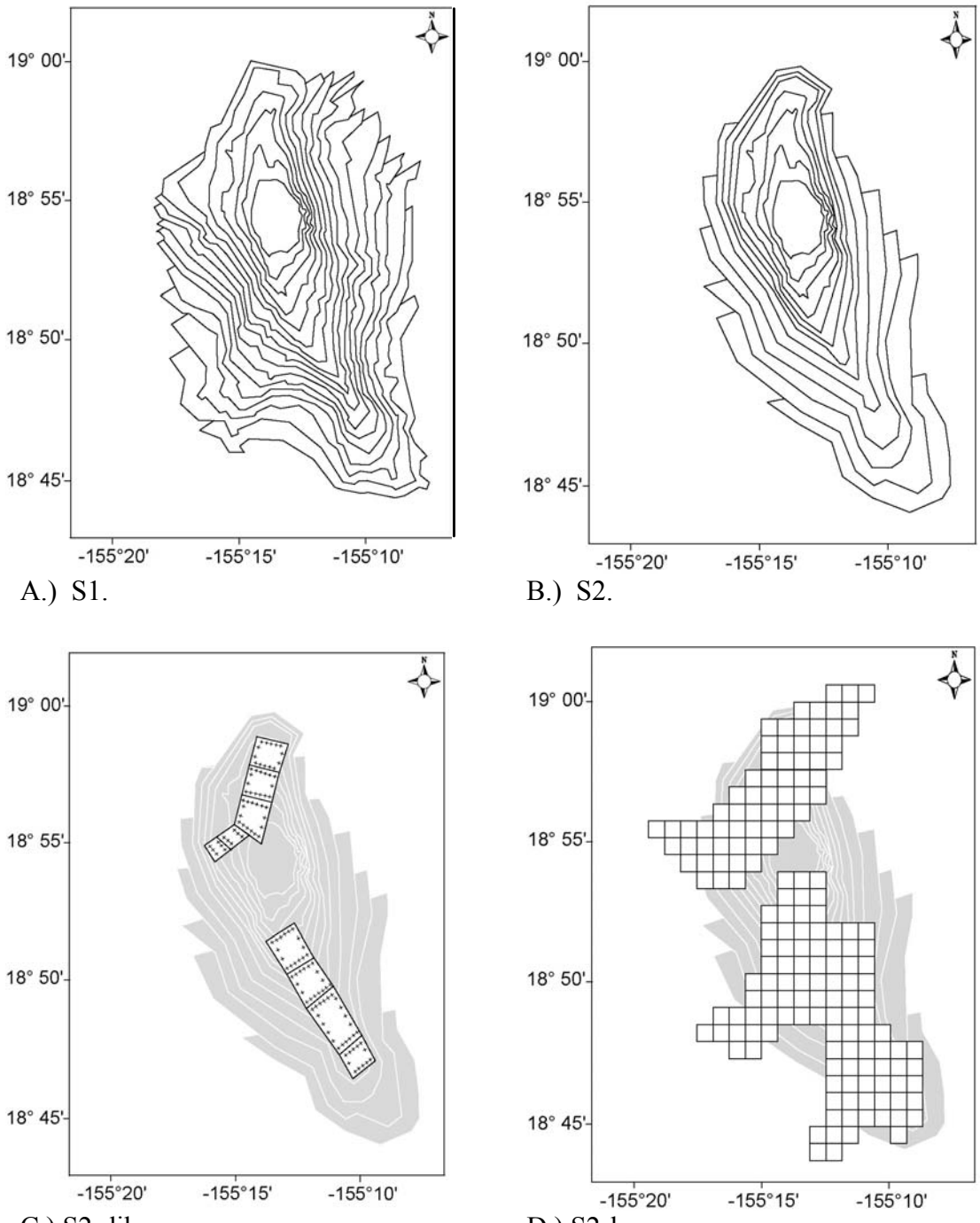

Figure 13. Polygon construction of first four models. A.) S1-homogenous model, B.) is S2-homogenous model, C.) includes the S2 model with the addition of dike complexes (S2-dike), and D.) includes the S2 model with the addition of lava flows (S2-lava).

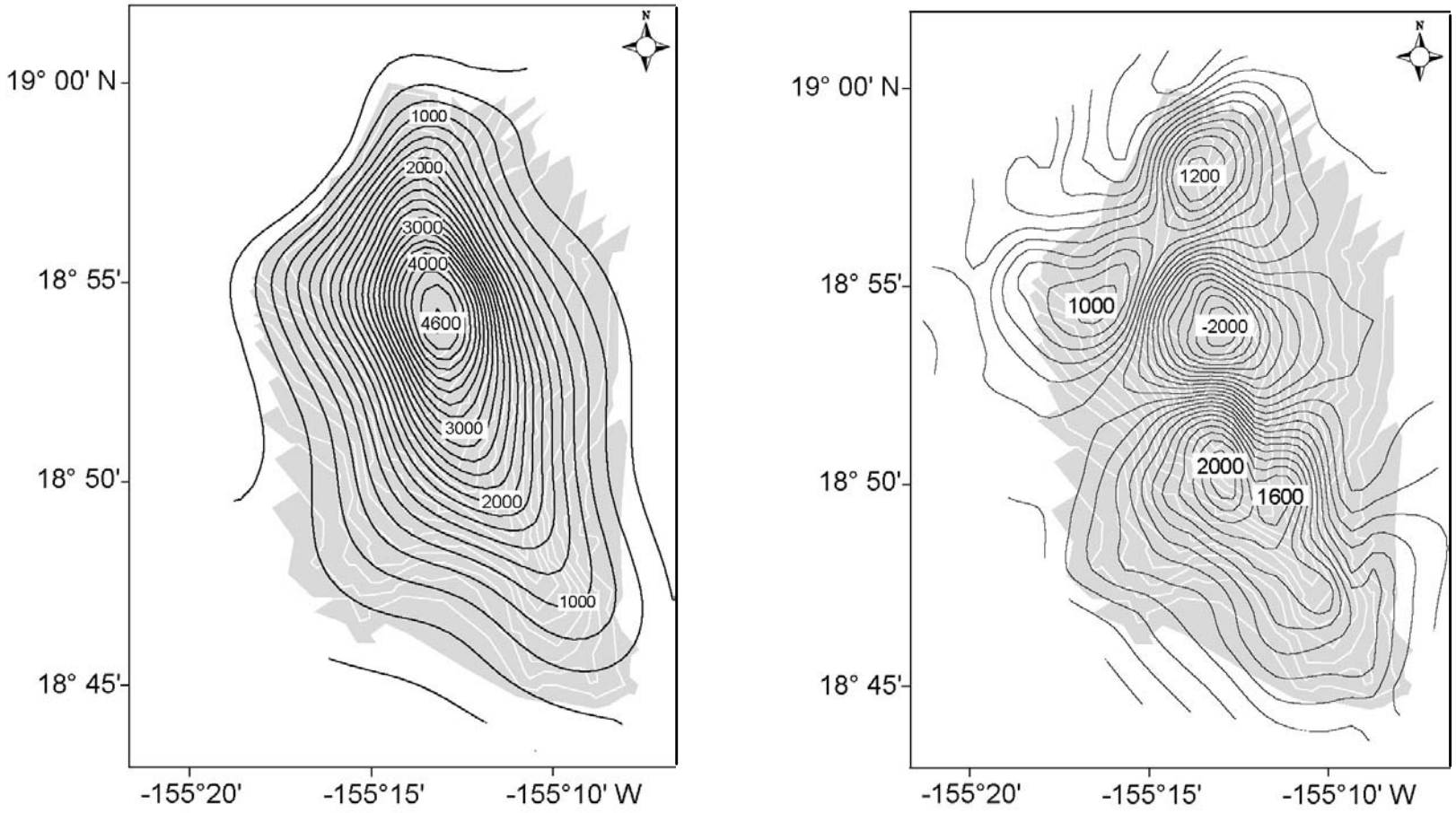

Figure 14. Calculated anomaly and residuals associated with the S1-homgenous body. The shape of the polygons are in gray. Note the extreme high and low residual values indicating that the observed magnetic field is not a simple function of bathymetry. Note how the maximum calculated anomaly is farther north, centered over the summit, than the observed (Fig. 8). Contour interval is 200 nT and polygon layers are outlined in white for reference.

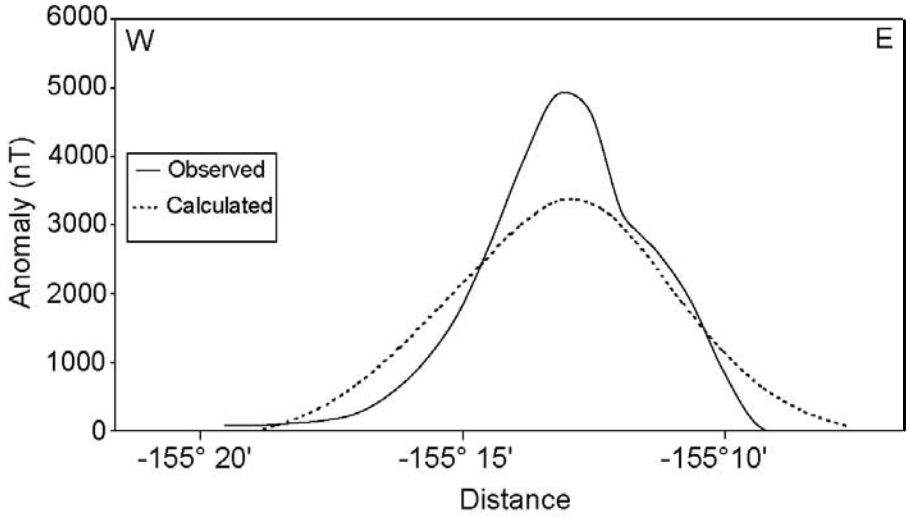

Figure 15. A profile of the calculated and observed magnetic anomaly along an EW transect at 18˚53' N. The calculated anomaly is wider than the observed and therefore the least-squares solution will not "fill" the observed peak.

Table 3. Results for model solutions.

Model	GFR	RMS (nT)	Shield Magnetization (A/m)	Anomalous Magnetization (A/m)	Body Depth (km)
S1	1.17	1118	8.2		
S2	1.39	974	12.65		
S2-dike	2.19	599	12.79	north = 55.66 south = 138.18	
S2-lava	2.28	563	12.35	north = 67.51 south = 81.00	
S2-nonmagnetic	2.29	571	22.64	-36.23	2.0 - 4.5
S2-anomalous bodies	4.37	305	24.44	a = 51.90	2.4 - 3.4
				b = 84.73	3.4 - 4.4
				c = -15.22	2.0 - 4.5
				d = 45.50	1.2 - 2.0
				e = -0.91	2.6 - 3.6
				f = 86.69	3.0 - 4.0
				g = 86.69	3.0 - 4.0
				h = 86.69	3.4 – 4.4
S3-anomalous bodies	4.54	289	23.59	a = 54.83	2.0 – 4.0
				b = 47.33	2.8 – 4.8
				c = 53.83	1.2 – 1.7
				d = -5.15	2.0 – 6.0
				e = -9.91	3.2 – 5.2
				f = 70.38	3.2 – 5.2
				g = 70.38	4.5 – 6.5
				h = 48.07	2.8 – 4.8
				i = 48.07	3.6 – 5.6
				j = 48.07	4.4 – 6.4
S1-anomalous bodies	4.17	303	25.40	a = 44.36	2.4 – 4.4
				b = 38.98	3.0 – 5.0
				c = 38.98	2.2 – 4.2
				d = 65.78	1.2 – 1.7
				e = - 4.95	1.7 – 7.5
				f = - 5.44	3.4 – 5.4
				g = -5.44	1.8 – 3.8
				h = 48.07	2.8 – 4.8
				i = 48.07	3.6 – 5.6
				j = 48.07	4.4 – 6.4

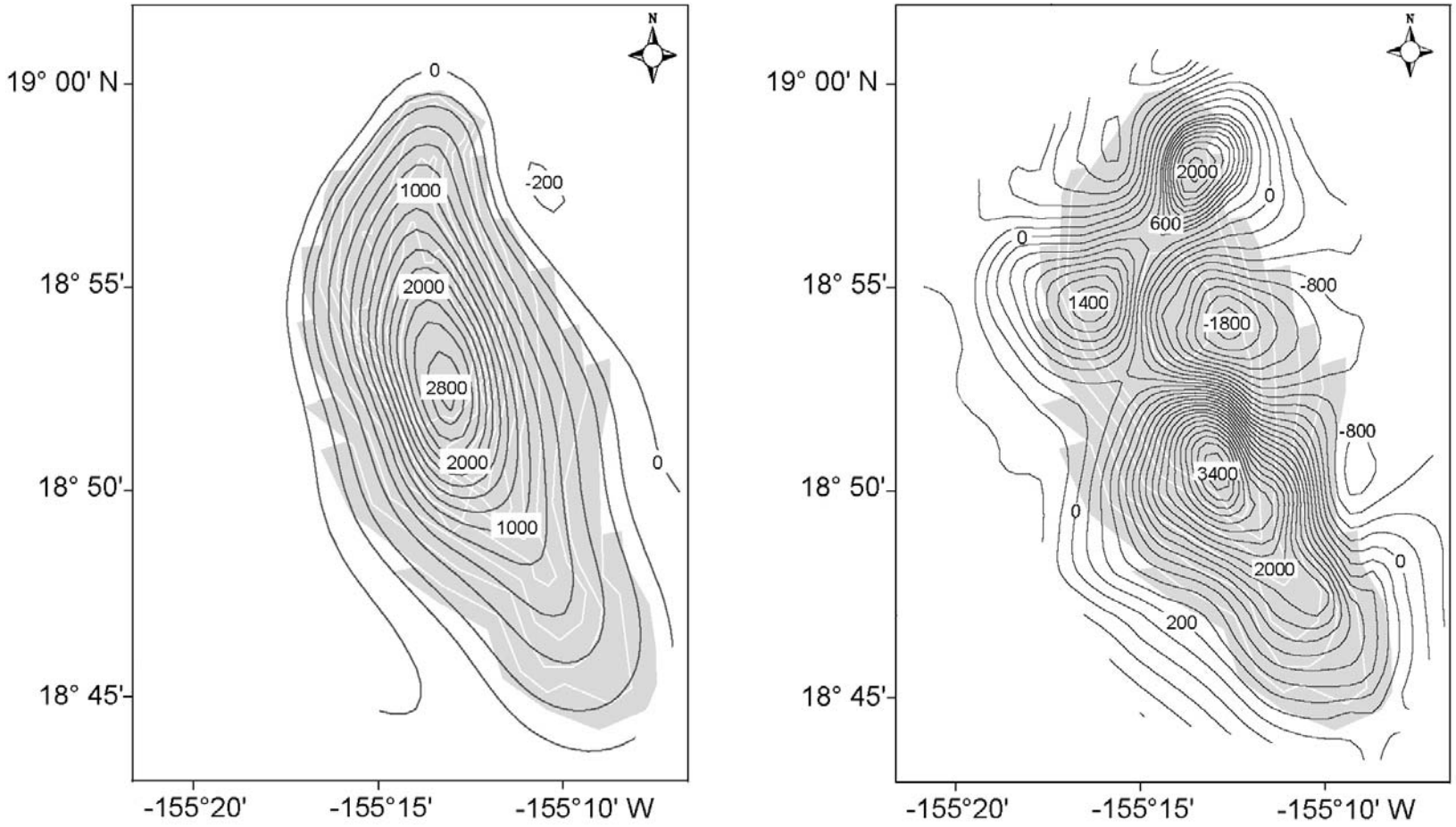

Figure 16. S2-homogenous model calculated and residual anomalies. The contours are at 200 nT intervals and the polygonal layers are outlined in white for reference.

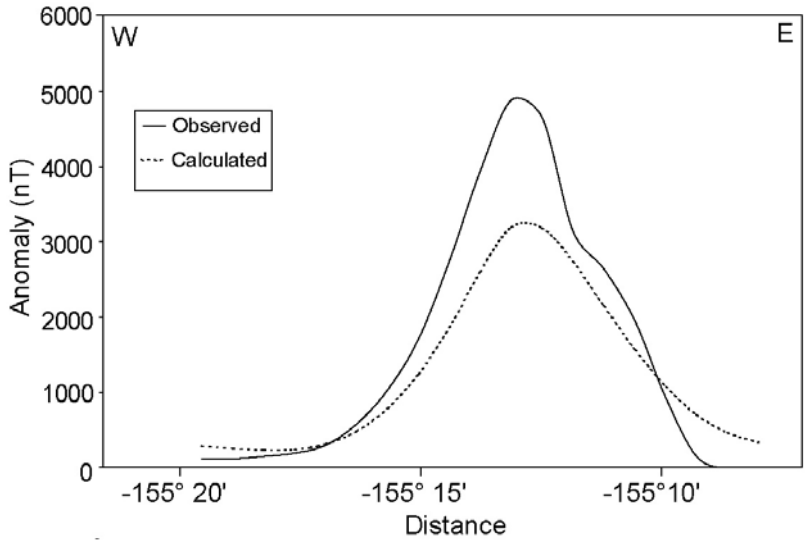

Figure 17. A profile of the calculated and observed magnetic anomaly of the S2-homogenous model along NS transect at 18˚53' N.

S2-Dike Model

Dike complexes are thought to be common within active seamounts. Therefore, dike complexes (S2-dike) are constructed in the form of rectangular blocks along the areas of high magnetization located on the north and south rift zone ridges using the magnetic anomaly map and the Fourier inversion solution as a guide (See Fig. 13). Tops are located just below the seafloor and trials were run with different bottom depths to discover the best fitting dike shape. First, the thickness of the dikes are varied with the blocks closest to the summit 2 km in thickness at both the north and south rift ridges with the next closest blocks 1.5 km thick and the remaining dikes at 1 km thick. This tapered dike model still leaves high residuals. On the edge of the block closest to the summit on the north rift ridge, a dipole residual with a low of –2200 nT and a high of 2000 nT lingers.

Similar residuals are present over the south rift ridge, again close to the summit, with a low of –1500 nT and a high of 3500 nT. Next, a constant bottom depth for all dike bodies was tried. The residuals varied only slightly in both intensity and location from the previous trial results. The last attempt in running the dike model consisted of the blocks being of constant thickness of 1 km. This model gives the least residuals although the fit is not substantially better and high residuals remained. The high dipole anomaly residuals are lowered slightly (Fig. 18) with the north values ranging from –1000 nT to 1600 nT and the north values from –1200 nT to 3000 nT. The main problems with this model is that the summit peak is too far south in the calculated anomaly, the shield magnetization is low at 12.79 A/m which is only about half of the measured rock properties average, and the south dike has a very high magnetization of 138 A/m.

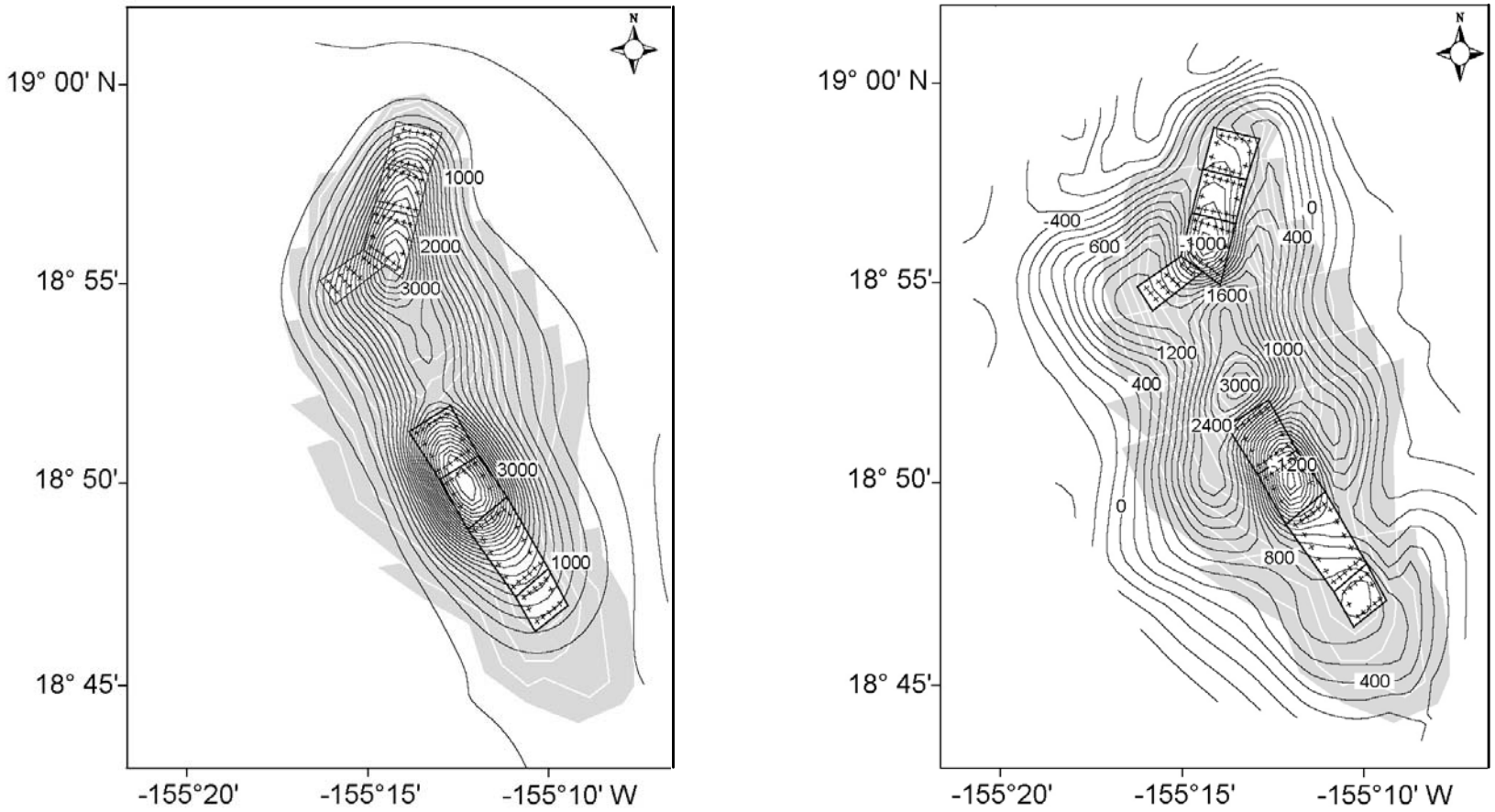

Figure 18. Calculated and residual anomalies of S2-dike model. Dikes are outlined in black on the north and south rift zones ridges. Two high, dipole residuals, one over the north rift ridge and the other over the south, are the reasons this model was considered unsatisfactory. For reference, the polygonal layers are outlined in white and the contour interval is 200 nT.

S2-Lava Flow Model

For this model, squares approximately 1 km^2, are constructed and constituted the upper 400 m of the north and south rift ridge areas (S2-lava). The location of both flows follow the magnetically high areas in the Fourier inversion magnetization solution. The idea behind this model is to follow the lobate structure of the observed anomaly and to test the hypothesis that highly magnetic, fresh flows on the rift zone ridges and upper flanks could cause the large anomaly highs. Modifications of the lava flow include reducing the area and varying the thickness. The best fitting modification (See Fig.13) gives the magnetization of the north flow at 67.51 A/m, the south is 81.00 A/m, and shield magnetization is low at approximately 12.33 A/m. Residuals over the north and south flow remain high (Fig. 19) and can not be reduced sufficiently. The GFR was 2.28 and the RMS was 563 nT. These results indicate that even with large thicknesses and magnetizations, the lava flows represent a volume that is too small to explain the large magnetic highs over the rift zone ridges.

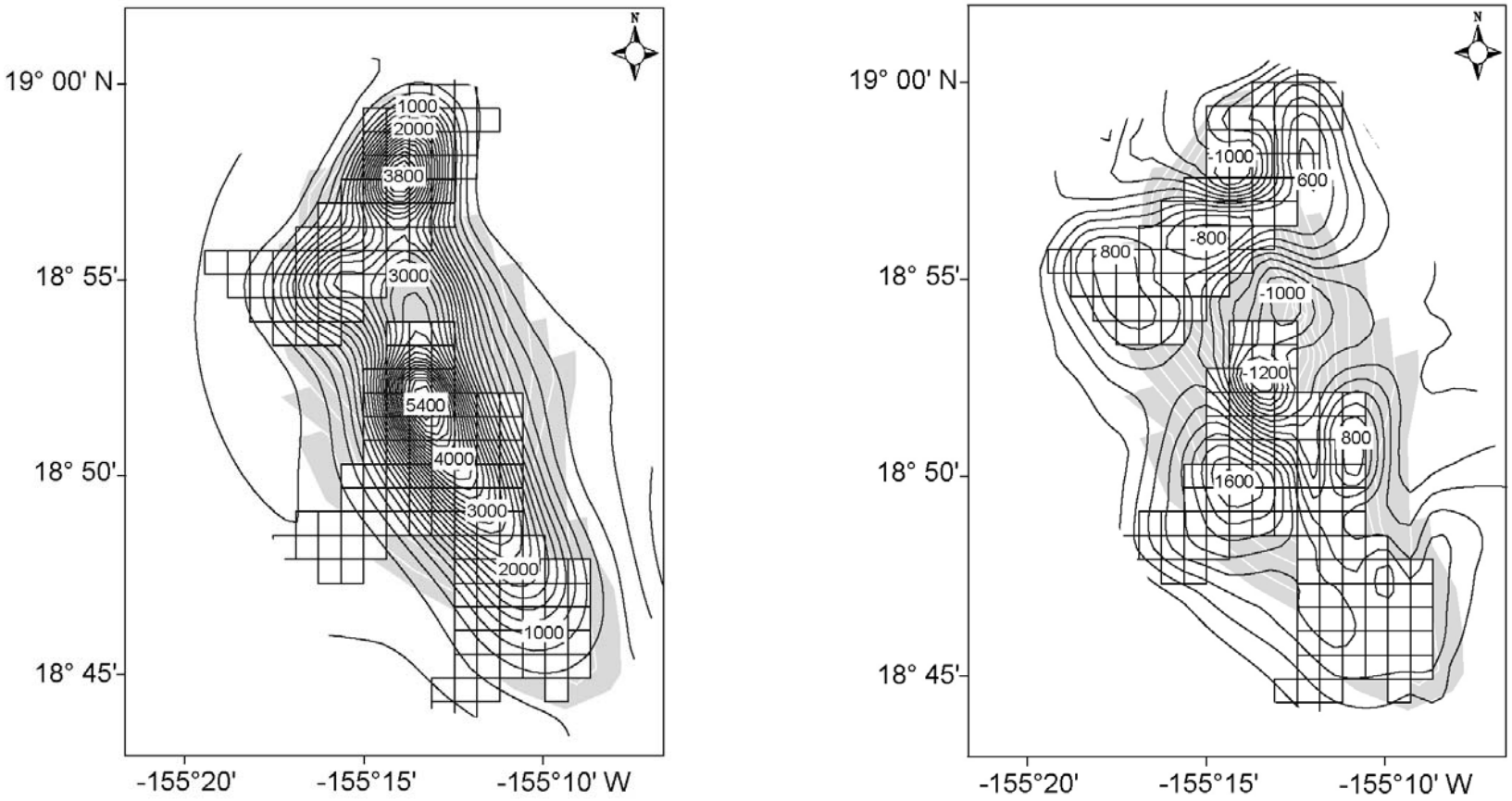

Figure 19. S2-lava flow model. The gridded squares representing flows over the north and south rift zone ridges are outlined in black. The contour interval is 200 nT. The polygonal interval is 200 nT. The polygonal layers are outlined in white for reference.

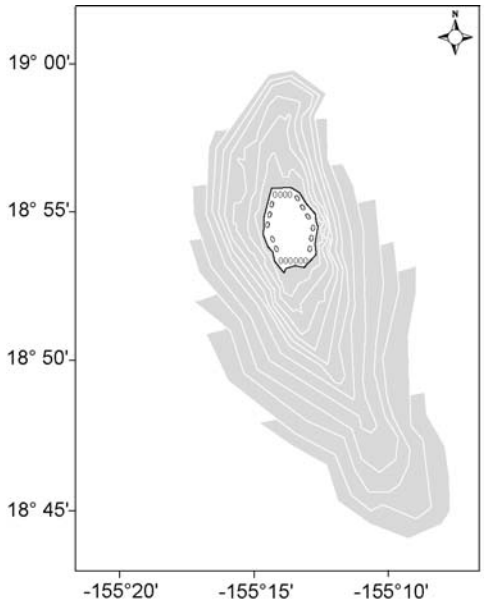

A.) S2-nonmagnetic.

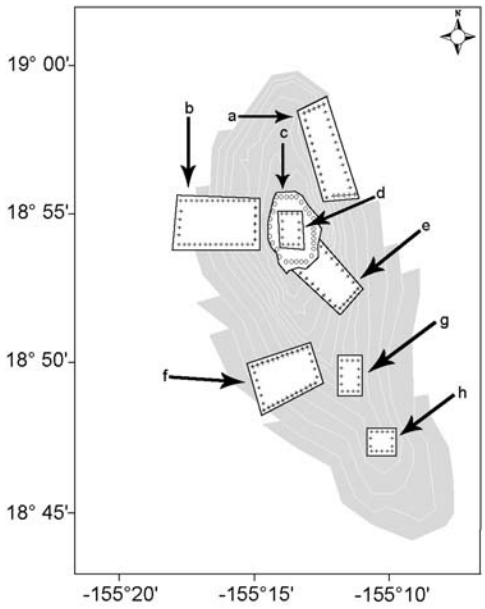

B.) S2-anomalous bodies.

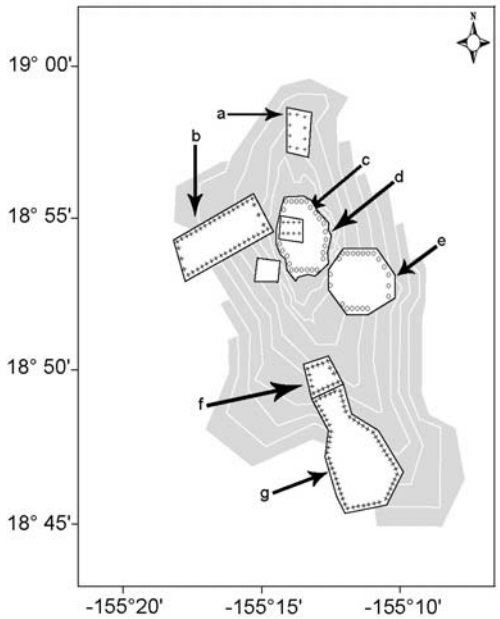

C.) S3-anomalous bodies.

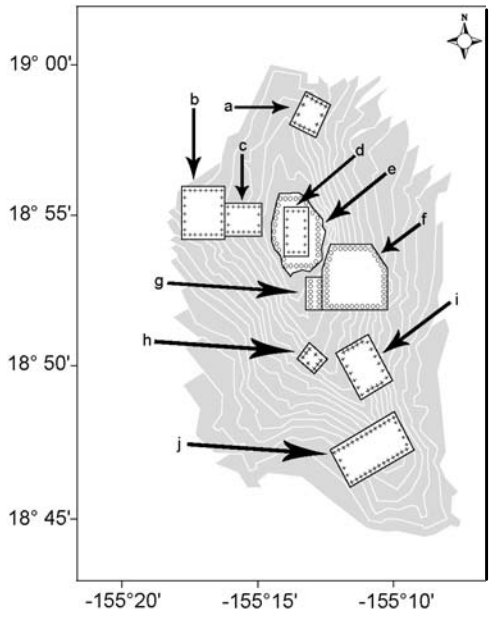

D.) S1-anomalous bodies.

Figure 20. Polygon construction of last four models. A.) S2 shield with a nonmagnetic summit, B.) S2 shield with anomalous bodies, C.) S3 shield with anomalous bodies, and D.) S1-anomalous uses the original approximation with anomalous bodies.

S2-Nonmagnetic Summit Model

The homogenous model makes an anomaly peak centered over the summit, but the observed anomaly peaks south of the summit. To reduce the anomaly over the summit, a nonmagnetic body representing a magma chamber and surrounding hot rock is constructed by following the 1200 m summit bathymetric contour with its top at a depth of 2 km below the surface and extending down to 4.5 km (Fig. 20). The summit anomaly is successfully reduced (Fig. 21) and provides a better approximation of the NS observed anomaly shape by canceling the anomaly at the summit and allowing the shield anomaly to grow in order to better fit the large anomaly on the south rift ridge (Fig. 22). However, the solution calculates a magnetization amplitude of –36.23 A/m, which is greater than the desired value. The desired value the negative magnetization of the shield. The calculated amplitude is therefore not a good approximation of a nonmagnetic body (see Table 3). A low GFR of 2.29 and a high RMS misfit of 571 are caused by the flanks and rift zone ridges still leaving high residual anomalies, although they are more restricted than before. With the magnetization amplitude and the residuals over the flanks still to be addressed, the nonmagnetic summit body is returned into our succeeding model.

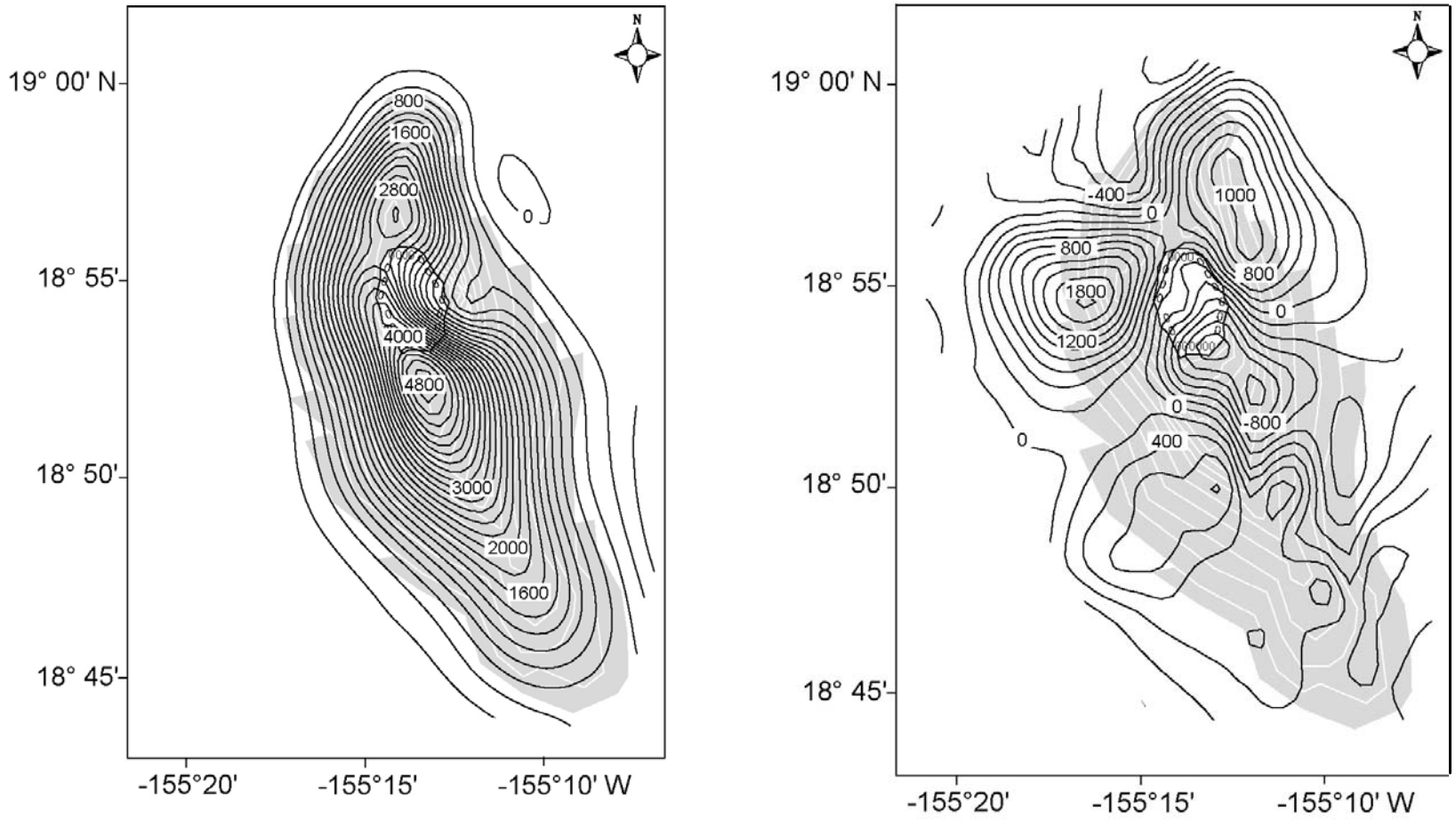

Figure 21. The S2-nonmagnetic summit model. The model was constructed by inserting a nonmagnetic block, outlined in black, within the seamount. The polygonal layers are outlined in white and the contour interval is 200 nT.

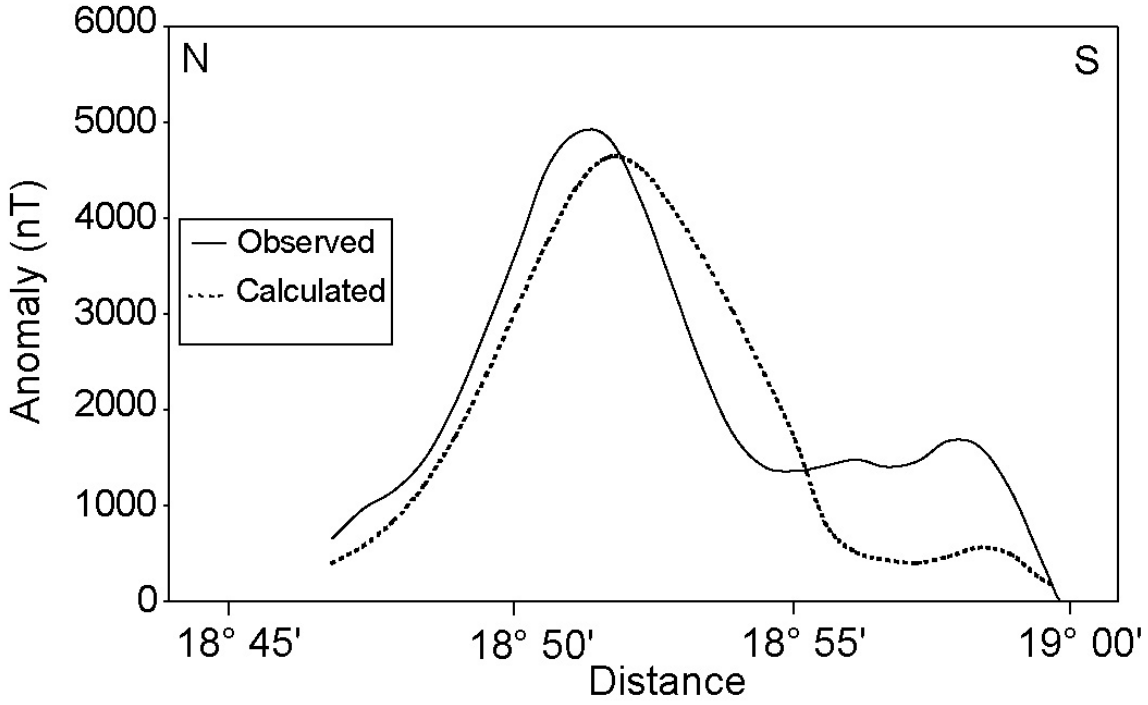

Figure 22. A profile of the calculated and observed magnetic anomaly of the nonmagnetic summit model (S2-nonmagnetic) along NS profile at 155˚12' W.

S2-Anomalous Bodies Model

Eight anomalous bodies are placed in the areas of remaining high residuals (S2-anomalous bodies model). Bodies with a positive magnetization were placed beneath positive residuals, to the east of the north rift ridge, within the summit contour, west of the south rift ridge, and two are placed along the south rift ridge and are labeled a-h (See Fig. 20). Two negatively magnetized bodies (c and e) are put south of the summit, in contact with, but not overlapping, the previous nonmagnetic body from the previous model. This solution produces residuals as low as 0 – 400 nT (Fig. 23), yielded a high GFR of 4.37, a low RMS misfit of 305 nT (see Table 3), and a wavelength that closely matched the observed (Fig. 24).

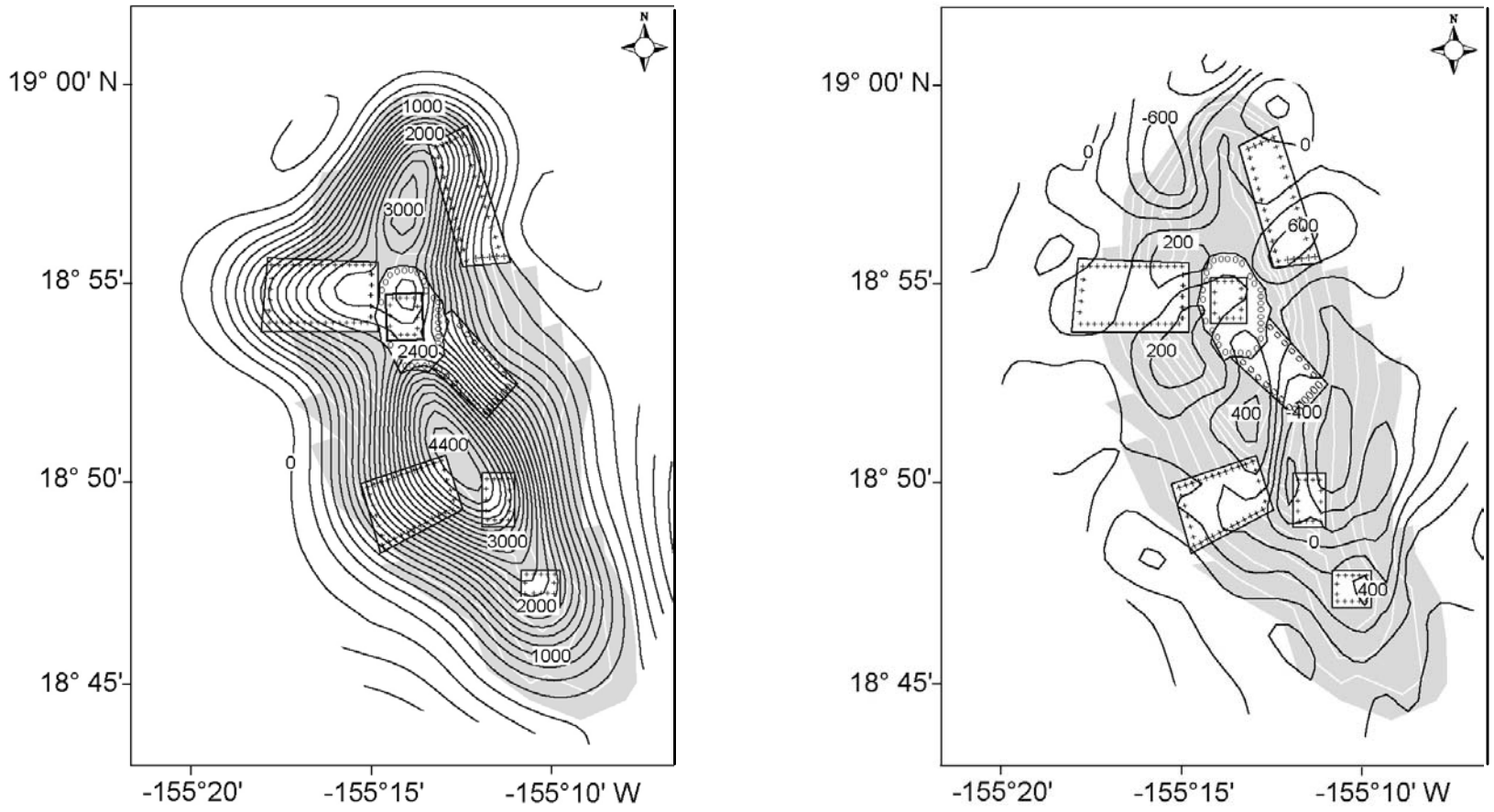

Figure 23. Calculated anomaly and residuals of the S2-anomalous bodies model. This model consists of source bodies of both positive and negative nonmagnetic magnetizations. The source bodies are outlined in black. Contour interval is 200 nT.

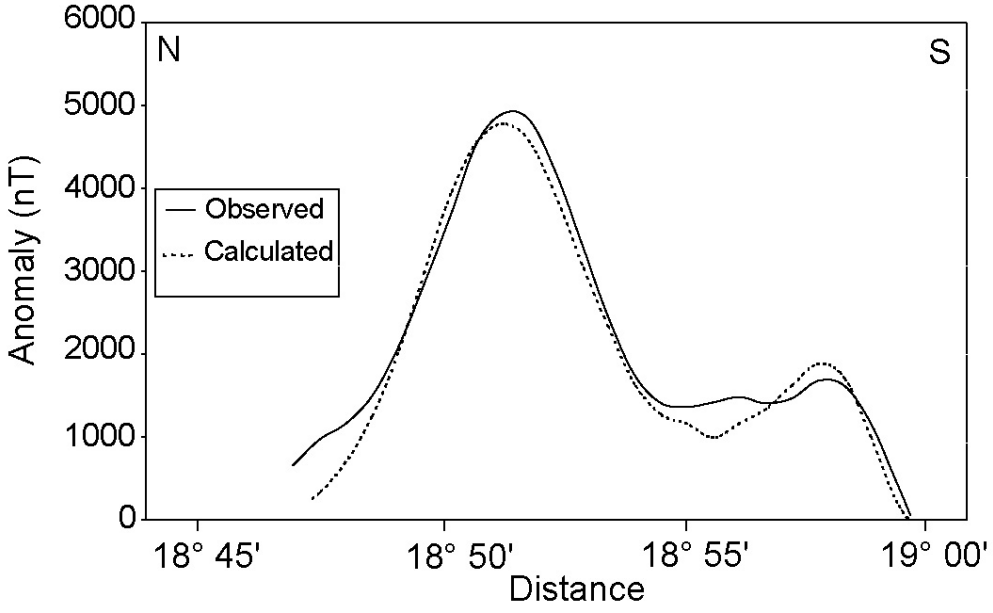

Figure 24. S2-anomalous bodies model along NS transect at 155˚12' W of the calculated and observed magnetic anomaly.

S3-Anomalous Bodies Model

This model includes flank ridges and was created by re-digitizing bathymetric contours which follows the steeper gradient between valleys and ridges. The difference between S2 and S3 polygon approximation is that S3 does not cut away the ridges on the west flank (S3). Using the same technique as the previous raisin cookie model, first a homogenous magnetization is assumed and then six anomalous bodies were placed in the areas of remaining high residuals with positive magnetizations beneath positive residuals to the east of the north rift ridge, within the summit contour, west of the summit, west of the south rift ridge, and two are placed along the south rift ridge and are labeled a,b,c,f,g, respectively (See Fig. 20). Two negatively magnetized bodies are put south of the summit (d and e), in contact with, but not overlapping, the previous nonmagnetic body from the previous model. This solution has residuals ranging as high as 600 nT (Fig. 25), yields the best fit of 4.54 (Fig. 26), and the lowest RMS misfit of 289 nT (see Table 3).

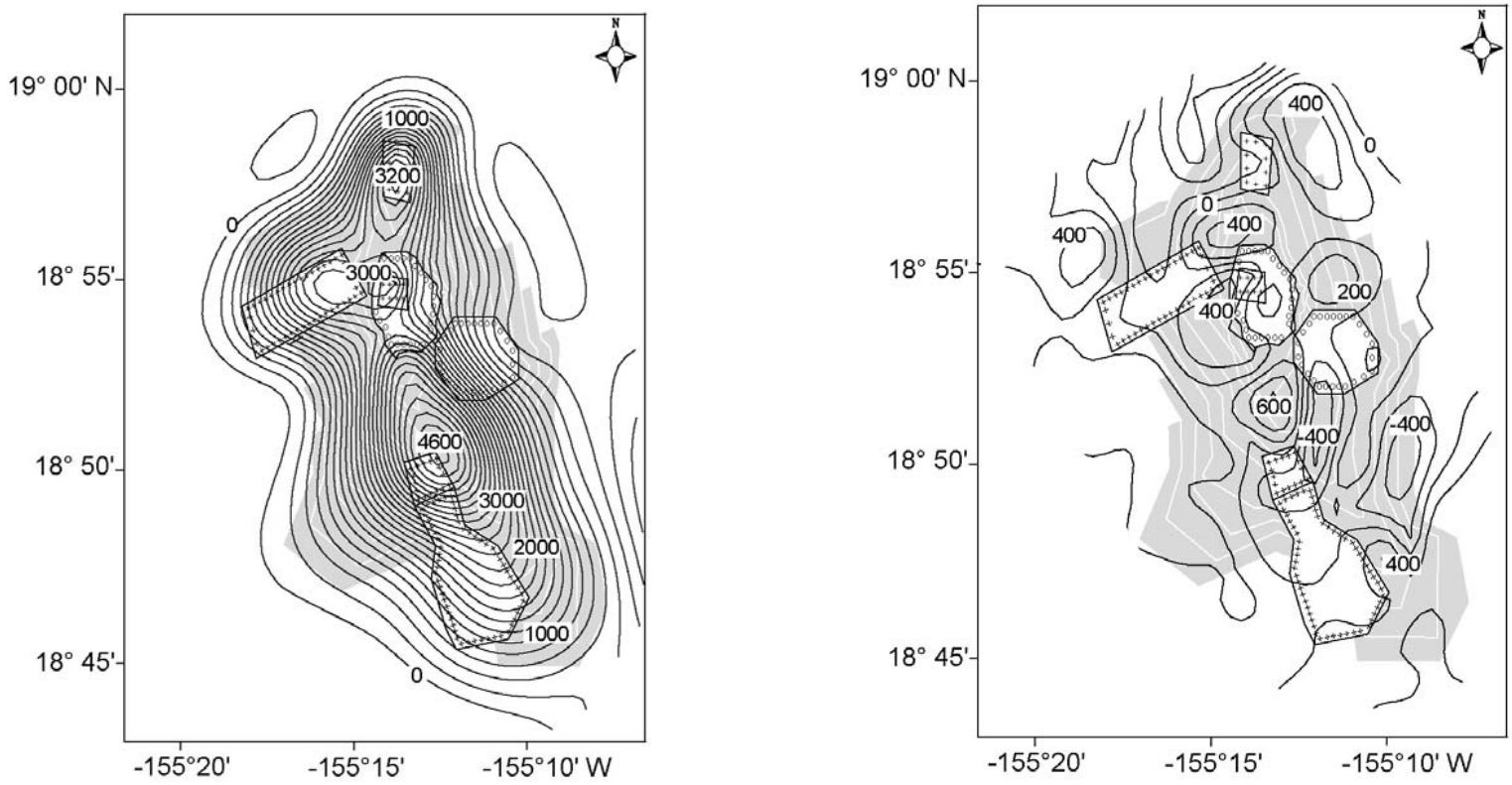

Figure 25. Calculated anomaly and residuals of the S3-anomalous bodies model. This model consists of source bodies of both positive and nonmagnetic magnetizations. The source bodies are outlined in black. Contour interval is 200 nT.

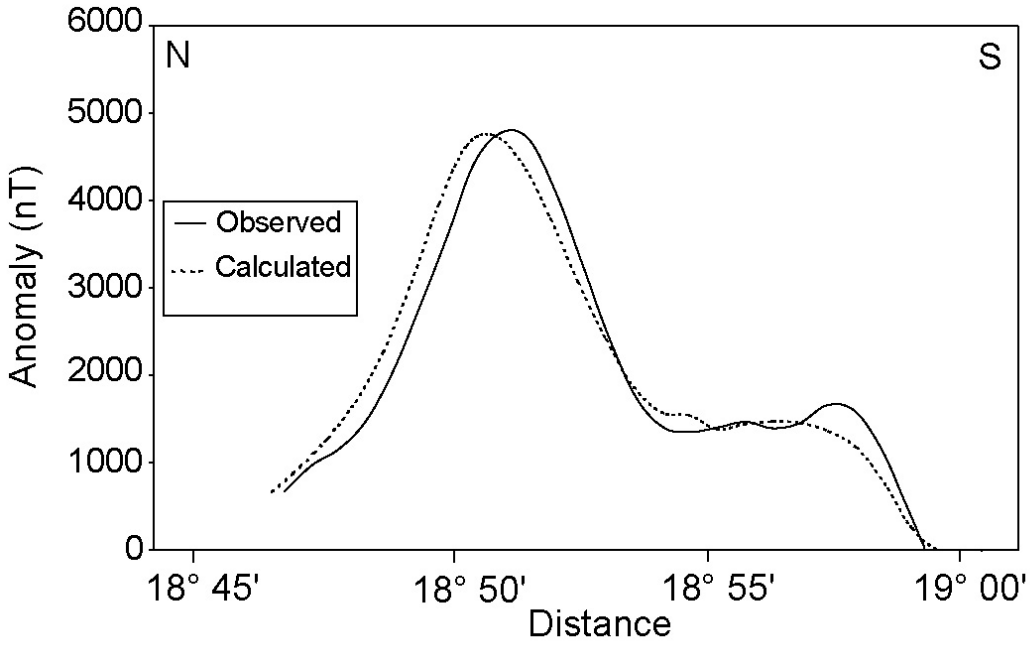

Figure 26. S3-anomalous bodies profile along NS transect at 155˚12' W of the calculated and observed magnetic anomaly.

S1-Anomalous Bodies Model

Although the S2-anomalous bodies model produced desirable results, it suggested a large amount of talus of considerable thickness dominates Loihi's anomalous field and does not include west ridges, which are likely to have a large affect on the magnetic structure. S3- anomalous bodies model accounts for more of the west ridges but cut away too much between the SW ridge and south rift ridge. This model returns to the original shield approximation, which does not assume slope shape. Nine anomalous bodies (a-i) are placed in areas of high residuals (See Fig. 20) from the previously run homogenous model (S1-raisin). Bodies with a positive magnetization were placed over the north rift ridge, west flank, three over the south rift ridge, and one over the summit (a, b, d, f, g, and h). The remaining three bodies were nonmagnetic, one located within the summit and two just south of the summit (c and e). This solution produces low residuals (Fig. 27), has a GFR of 4.17, a RMS misfit of 303 (See Table 3), and closely fits the observed wavelength (Fig. 28). The quality indicators are not quite as good as the previous model by 0.05%. This percentage is not significant and this model uses one less assumption (slope shape) and is therefore thought to be a more believable solution.

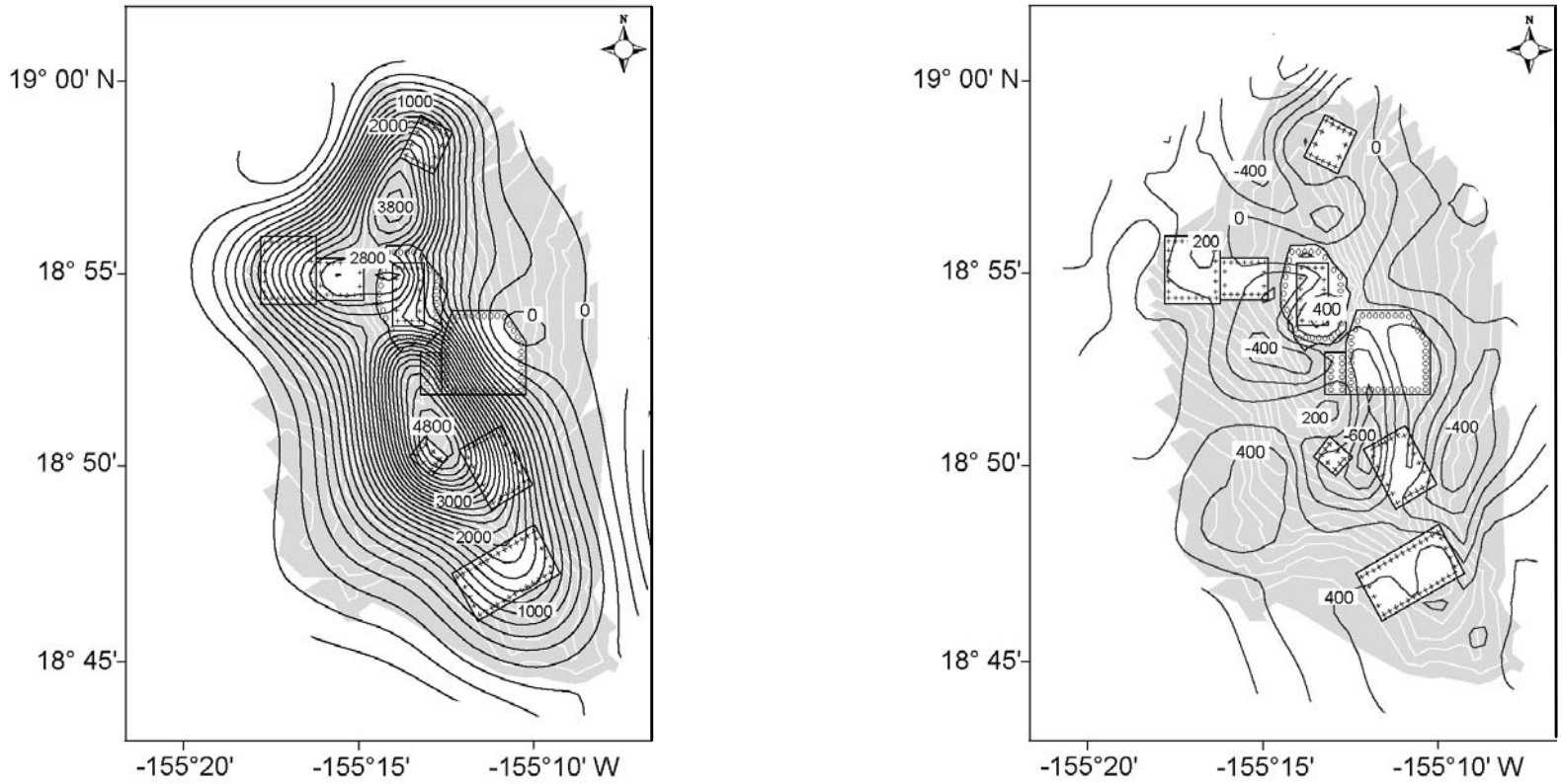

Figure 27. Calculated anomaly and residuals of the S1-anomalous bodies model. This model consists of source bodies of both positive and nonmagnetic magnetizations. The source bodies are outlined in black. The contour interval is 200 nT.

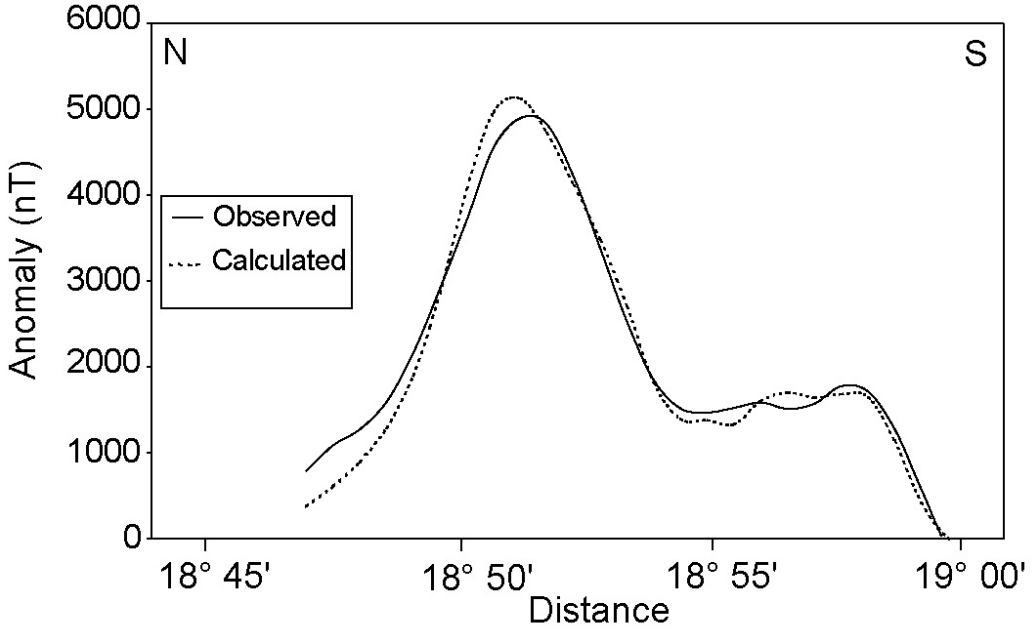

Figure 28. S1-anomalous bodies model along NS transect at 155˚12' W of the calculated and observed magnetic anomaly.

DISCUSSION

Rock magnetic property results and modeling solutions have demonstrated that a complex anomalous field exists over Loihi Seamount. The NRM of Loihi samples provide an estimation of magnetization magnitude and various models have been constructed to approximate the observed magnetic field. A number of source bodies and volcanic processes are suggested from the results of this study and are discussed below.

Magnetic intensities from rock samples are widely varied. Variable rock properties have been reported on active seamounts with NRM intensities ranging from 0.06 - 130 A/m (Tivey and Johnson, 1990; Tivey, 1994; Gee et al., 1989). The results produced in this study also display a wide range, but are generally stronger ranging from 1-157 A/m. The high magnetizations are characteristic of newly erupted basalts and the low magnetizations may be produced from demagnetization with age, hydrothermal alteration, and/or results from mass-wasting events.

The three-dimensional Fourier magnetization inversion demonstrates the effect of varying horizontal magnetization as a source for observed anomalies. A comparison of the Fourier solution with the final model construction (S1-anomalous bodies) shows that the Fourier solution and S1-anomalous bodies model produces similar anomaly highs and lows (Fig. 29). Magnetic highs correspond to bathymetric highs. The inverted "y" previously observed over the north rift ridge in the RTP anomaly is again produced in the Fourier solution. Steep amphitheater valleys and talus debris have been reported to be common features of Loihi's flank (Malahoff, 1987; Fourari et al., 1988). Two

obvious valleys are located on the west flank in addition to another on the east flank and are also visible in the bathymetry, RTP anomaly, and by anomalous Fourier lows (See Fig. 29).

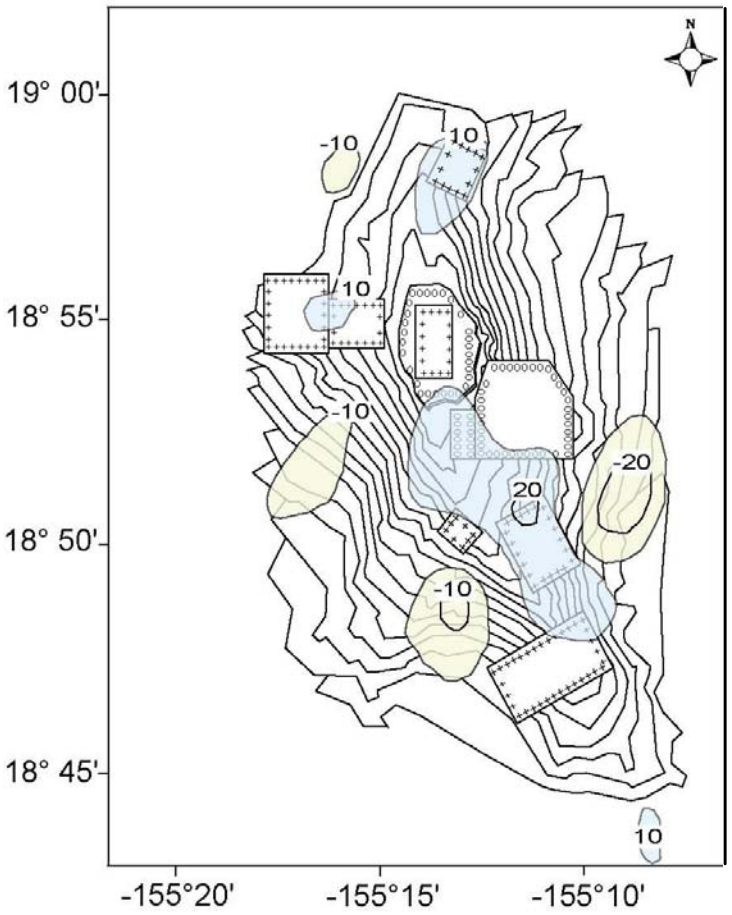

Figure 29. Comparison of S1-homogenous anomalous bodies and Fourier inversion solution. Polygon approximation and anomalous bodies are white, positive Fourier solution areas are tinted in blue, and negative areas are in yellow.

Because the Fourier solution is unbiased, it is an important starting point in modeling Loihi's magnetic structure. More specifically, the Fourier solution produces magnetic lows over the basal flanks, probably due to the constant thickness assumption which is

most likely not representative of Loihi's geology and therefore not a good approximation of Loihi's structure. Another reason that the constant thickness assumption may not be a good approximation is because it produces a deep, zero magnetic body, which may cause one of the negative magnetizations and over the nonmagnetic body (Fig. 30). The close proximity of the base of the seamount to the surface creates a narrower wavelength whereas a sloped bottom, used in the forward and inverse models, produces a broader wavelength. The apparent success of S2-anomalous bodies model and the skinny rift S3-anomalous bodies model is therefore consistent with the Fourier solution for these reasons and correspond to geological evidence of reports that mass-wasting events along the flanks of oceanic shield volcanoes is a major process during growth (Holocomb and Searle, 1991; Moore et al., 1994). Nevertheless, deposits from mass wasting events would need to be of considerable thickness in order to account for the large amount of narrowing in the S2 and S3 modifications. The high and low anomalies produced in the Fourier solution correspond to most of the anomalies in the conclusive inverse model (S3-anomalous bodies). However, several anomalies, especially at the summit, are not addressed with the Fourier inversion.

It is likely that the magnetic source layer of Loihi Seamount is intruded with dikes and sills that are both young and old (Fig. 31). Ultimately, the S2 an S3 modifications were not significantly better than the homogenous shield (S1) and they include an additional assumption about the shape of Loihi.

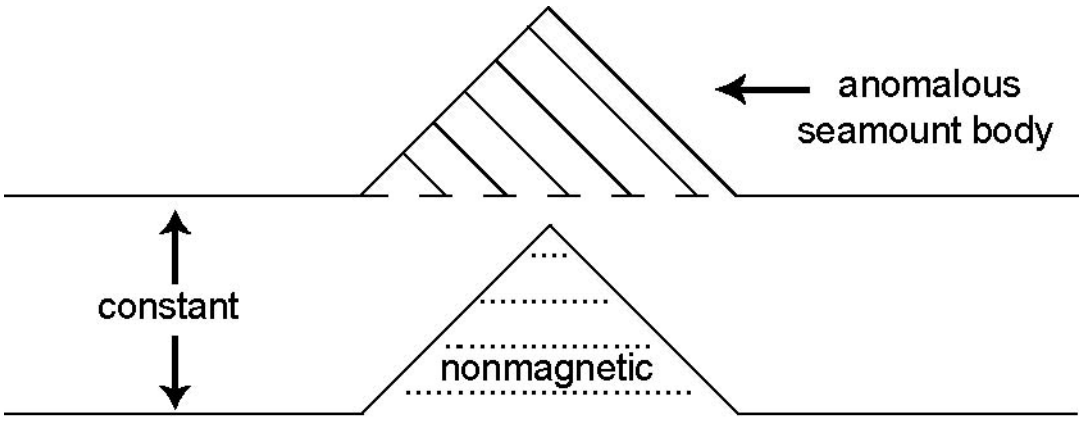

Figure 30. Schematic of Fourier inversion constant thickness assumption.

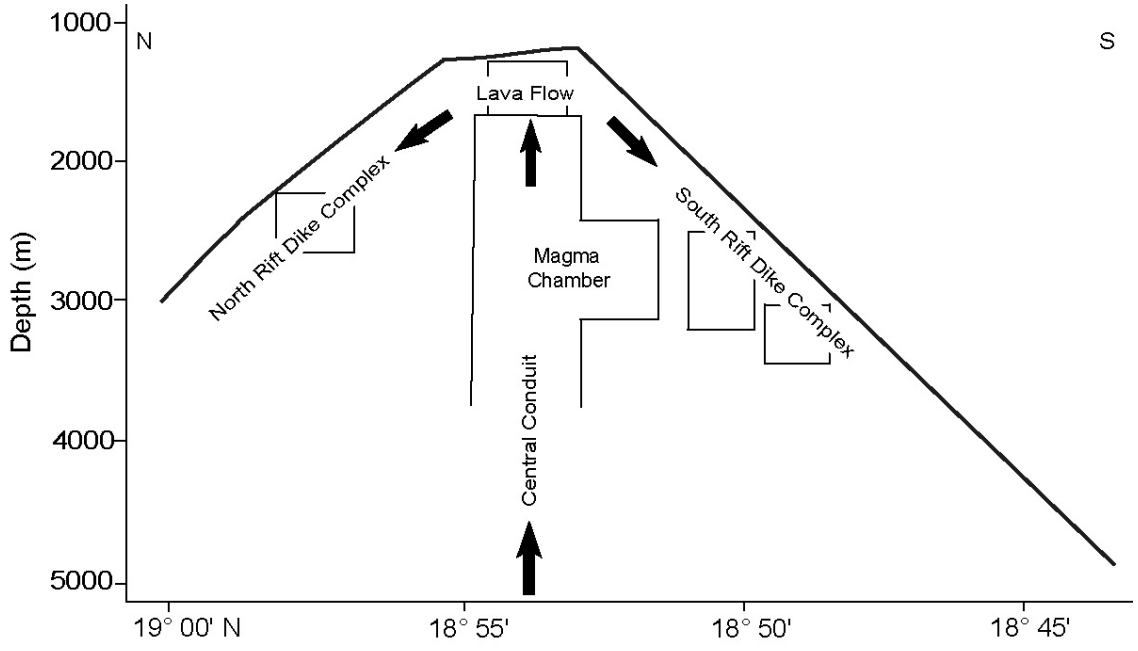

Figure 31. General schematic of proposed processes that create the horizontal magnetization variation in Loihi Seamount.

Contributing factors to horizontal variation within the magnetization could be geochemistry and hydrothermal variation. The process of basalt fractionation causes a higher iron and titanium content and thus higher intensities. Fractionated basalts have been observed on Loihi Seamount (Johnson and Clague, 1981). Hydrothermal activity has also been observed on Loihi. The circulation fluids may interact with the source rock and reduce the magnetization by breaking down the magnetic minerals (Irving, 1970; Johnson et al., 1982)

Loihi's summit has been deemed young and active by several investigations using underwater photography (Malahoff, 1987) geochemistry (Malahoff et al., 1982; Karl et al., 1988; Garcia et al., 1995; Guillou et al., 1995), and multi-beam bathymetry (Fornari 1988). A summit magma reservoir was previously postulated using magnetic modeling (Malahoff, 1987) and this study yields similar results. The nonmagnetic body within Loihi's summit is interpreted to be a central magma reservoir with hot nonmagnetic rock surrounding it. In all anomalous bodies model variants, there is a nonmagnetic zone present at the summit and an additional zone to its SE. A reasonable geological interpretation of this second nonmagnetic body is that it is part of a magma chamber and conduit. The conclusion of a magma chamber defined by anomaly low over the summit is similar to that reached of Axial Seamount (Tivey and Johnson, 1990), Gran Canaria Volcano (Blanco-Montenegro et al., 2003), and Kilauea Volcano (Hildenbrand, 1993). In addition the model implies a thin, small, highly magnetic body lies atop of the central nonmagnetic zone. Further evidence for the existence of the

above body comes from NRM intensity measurements in this area, which range from medium to high values (See Fig. 9). Newly erupted lavas have also been observed in this area (Malahoff, 1987) and therefore the highly magnetic body is interpreted as fresh, highly magnetic flows.

Several strongly magnetic source bodies are located throughout the seamount. Results from the dike and lava flow models suggest that the strongly magnetic bodies are not any one structure but most likely a combination. A magnetic high is located below the north rift zone ridge, another located beneath a ridge to the west of the summit, two below the south rift zone ridge, and one directly west of the south rift ridge. Active volcanoes are known to contain a large number of dike intrusions, especially in and near rift zone ridges. Therefore, the highly magnetic areas located on north, south, and the less prominent west rift ridge, are most likely dike intrusions. Dike intrusions along rift zone ridges are generally linear (Walker, 1999) and tend to be long, narrow, and straight within the Hawaiian shield volcanoes (Dietrich, 1988). The areas of intrusive rock occupy a large area and are also younger than surrounding rock causing a strong positive magnetic signature. Because the bodies must be relatively thick to mimic anomaly amplitudes, it is unlikely that the bodies are piles of fresh lava flows which are generally thinner. The reasoning for interpreting these structures as freshly intruded basalts is that similar findings, high magnetic anomalies in likely areas of intrusions, were found at Kilaeau Volcano (Hildenbrand, 1993), Gran Canaria Volcano (Blanco-Montenegro et al., 2003), and Reunion Volcano (Lenat et al., 2001).

The similarities of magnetic bodies in all of the anomalous models suggest that the existence of the bodies is a robust feature. However, the differences are an example of the nonuniqueness of magnetic modeling. Magnetic bodies over the north, west, and south rift ridges exist in all models and nonmagnetic bodies subsist over the summit and south of the summit. The type, extent, and positions of anomalous bodies are similar, but must be changed slightly to match the residual anomalies in the different models.

This investigation of Loihi's magnetic structure produces similar results with the previous study of Loihi's magnetic structure (Malahoff, 1987). Both indicate a complex magnetization, a nonmagnetic body at the summit, and an additional magnetic body at the center. The previous study is two-dimensional and therefore the additional magnetic body appears as a tube. This study is three-dimensional and the magnetic body is rectangular which has been already discussed.

The similarities produced between anomalous bodies models, Malahoff's previous investigation of Loihi's summit, and results from other active volcanoes were utilized to produce a geologic interpretation of Loihi (Fig. 32). The interpretation proposes a magma system and system at and south of the summit, rubble, and north, south, and west dike intrusions. Evidence for the magma system and dike intrusions has been previously discussed. It is important to note that each dike complex may consist of many separate dike intrusions, which is similar to what has been observed in other Hawaiian volcanoes (Walker, 1999). Indications of talus debris are anomalous lows, a noticeable bulge in the bathymetry contours, and reports that mass-wasting debris is extensive on Loihi's surface (Malahoff, 1987; Fourari et al., 1988).

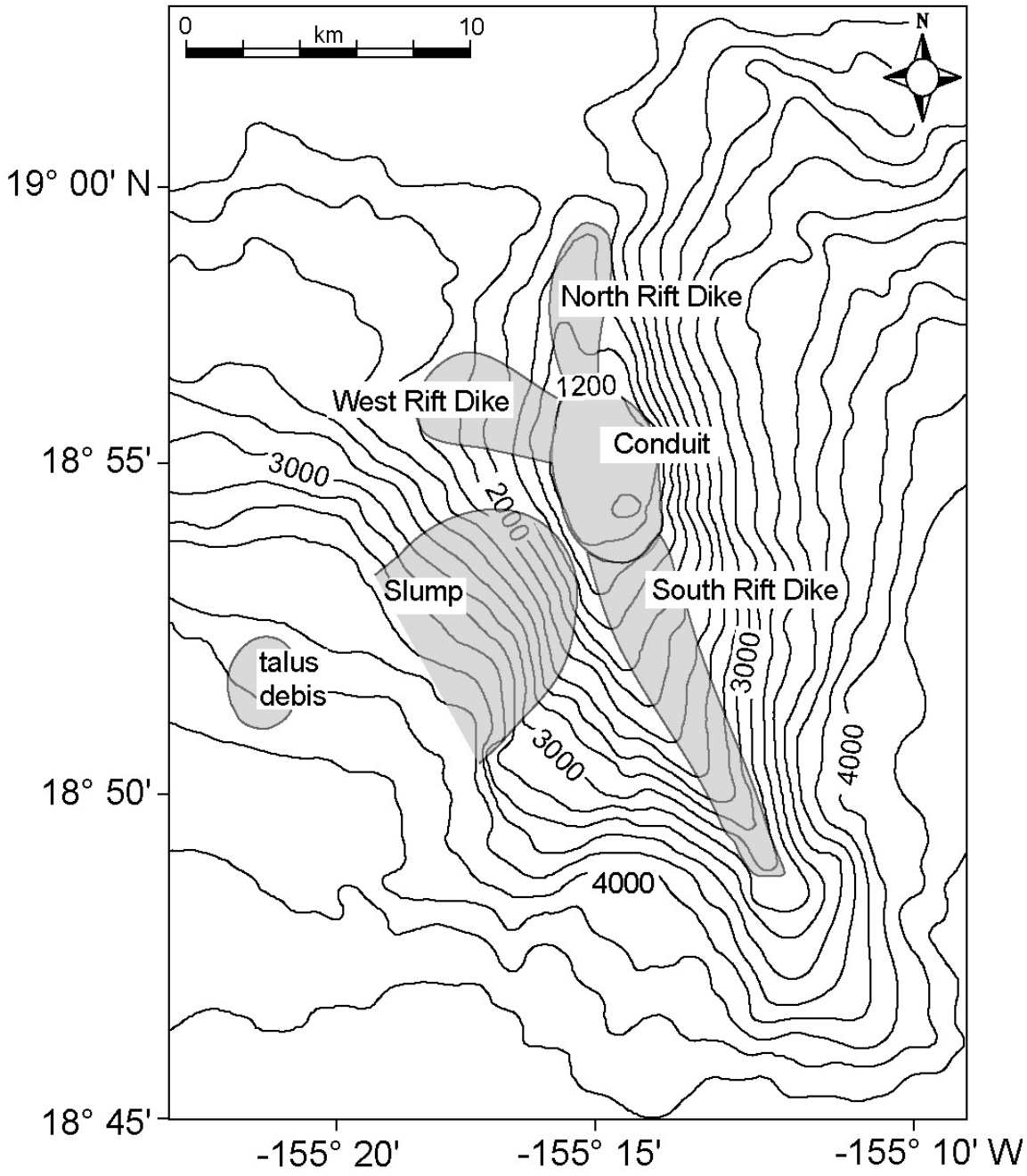

Figure 32. Geologic interpretation of Loihi Seamount.

Several caveats must be addressed when considering our model interpretation. Navigational errors and lack of regularly spaced magnetometer data are the first. Despite XOVER being used in order to correct navigational errors and data offsets, an average COE of 82 nT still persists, which means that some intersections have higher COE, with the highest of 410 nT. Areas where only one ship track from an older survey is present are further complicated by an unknown amount of navigational error due to lack of other ship tracks to compare it too. The compiled, corrected magnetic data was also gridded. The process of gridding can allow poorly positioned or corrected data to be interpolated into mis-located contours. In areas of steep gradient, the manual misplacement of a track could affect the anomaly field by up to ~2400 nT. However, these areas are generally well controlled by several survey tracks. A reasonable estimation of error in anomaly field contours caused by the misplacement of a track is ~200 nT which may cause subtle features (~1/2 km) to appear.

Magnetic modeling provides insights into approximate location and size of source bodies. The approximate source body location was determined using the anomalies from RTP transformation and their shape was adjusted to fit anomalous features. However, the lateral extent and depth are not well known. Source bodies could be larger or smaller depending on their actual magnetization. For example, an anomalous subsurface body with twice the magnetization but half the volume would create approximately the same anomaly. Therefore, the anomalous bodies used here are only an approximation of geology. Interpretations are put forth with regards to rock magnetic property results as well as sensible volcanic geology, that is, geology that is

common and realistic on and within active volcanoes. However, modeling cannot resolve small volcanic features, the exact location of features, or separate structures that may be near each other. An additional limitation of the modeling done in this study is that the computer program can only accept 5 or less anomalous bodies. Because the magnetic structure of Loihi is complex it is necessary to combine the magnetization field of two or more bodies which further generalizes the produced solutions. This was especially true for the S1-anomalous bodies model, which contained nine anomalous bodies. Undoubtedly further adjustments of the models could be made to achieve even better representations, but the incremented changes would not change the interpretations already made.

The relevance of the information provided by the rock samples should also be considered. All samples were taken close to or on the surface of the summit (See Fig. 5). These samples only characterize the surface of the summit area and do not represent the entire seamount edifice. Although we have no reason to think the samples are not representative, they only tell about surface flow magnetization.

CONCLUSIONS

Magnetic survey data from 12 different research cruises were combined, rock magnetic properties were investigated, and several modeling techniques were used to investigate the magnetic structure of Loihi Seamount, Hawaii. The magnetic anomaly map of Loihi Seamount shows a complex magnetic structure with strong magnetic highs over the north and south rift ridges. Rock samples were strongly magnetized with a mean intensity of 26 A/m. The final model for Loihi Seamount uses nine anomalous bodies, two nonmagnetic and seven highly magnetic, implicating several volcanic processes.

Observations of the magnetic anomaly map show that Loihi has a strongly magnetized shield with significant high and low anomalous areas. High anomalies are over the north and south rift ridges, the highest above the north most section of the south rift ridges. Low anomalies persist over the basal flanks of the volcano.

Recovered rock samples from Loihi Seamount also indicate that the seamount is strongly magnetic. The average NRM (26 A/m) and suceptibility (5.0×10^{-3}) are higher than other recorded values of Hawaiian oceanic basalt. Large Q ratios (up to 754) suggest that induced magnetization has little to do with the overall magnetization.

The Fourier Inversion solution provides an initial, unbiased approximation of the magnetic structure. Results show similar features to those in the RTP transformation including high magnetizations over the north and south flanks and low magnetizations

occur around the basal flanks. Several areas of high and low magnetization agree with the observed and S1-anomalous bodies magnetic field.

Forward models provide the location, approximate depth, and approximate strength of each anomalous body. Although there are slight variations, anomalous areas persist and the locations and sizes are robust.

Modeling of the magnetic anomaly show anomalous highs over the north and south rift zone ridges which are likely to be intrusive bodies and/or recently erupted lava flows, nonmagnetic zones at the summit and south of the summit probably part of a magma system, and surrounding low magnetization on the basal flanks of the seamounts perhaps due to be talus debris with a cumulative incoherent magnetization.

The complex magnetization results are characteristic of young, active volcanoes. This study produces similar findings to the previous investigation of Loihi Seamount, active Axial Seamount, as well as other active volcanoes such as Kilauea.

REFERENCES

Bhattacharyya, B. K., Two dimensional harmonic analysis as a tool for magnetic interpretation, *Geophysics, 30*, 829-857, 1965.

Blanco-Montenegro, I., J., A. Torta, M. Garcia, and V. Arana, Analysis and modeling of the aeromagnetic anomalies of Gran Canaria (Canary Islands), *Earth Planet. Sci. Lett., 206*, 601-616, 2003.

Bonatti, E., Mechanisms of deep-sea volcanism in the South Pacific, *Res. Geochem., 2*, 453-491, 1967.

Clague, D. and G. B. Dalrymple, Tectonic, geochronology, and origin of the Hawaiian-Emperor volcanic chain, in *The Eastern Pacific Ocean and Hawaii, The Geology of North America,* edited by E. K. Winterer, D. M. Hussong, and R. W. Decker, vol. N, pp. 188-217, Geological Society of America, Boulder, Colo., 1989.

Dieterich, J., Growth and persistence of Hawaiian volcanic rift zones, *J. Geophys. Res., 93,* 4258-4270, 1988.

Fornari, D. J., M. Garcia, R. Tyce and D. Gallo, Morphology and structure of Loihi Seamount based on seabeam sonar mapping*, J. Geophys. Res., 93*, 15,227-15,238, 1988.

Frey, F. A. and D. A. Clague., Geochemistry of diverse basalt types from Loihi Seamount, Hawaii: Petrogenetic implications, *Earth Planet. Sci. Lett., 66*, 337-355, 1983.

Furumoto, A. S., Nature of the magma conduit under the East Rift Zone of Kilauea Volcano, Hawaii, *Bull. Volcanol., 41-4*, 435-453, 1978.

Garcia, M. O., D. Foss, H. B. West, and J. Mahoney, Geochemical and isotopic evolution of Loihi Volcano, Hawaii, *J. Petrol., 36*, 1647-1674, 1995.

Gee, J., H. Staudigel, and L. Tauxe, Contribution of induced magnetization to magnetization of seamounts, *Nature, 342*, 170-173, 1989.

Gee, J., L. Tauxe, J. Hildebrand, H. Staudigel, and P. Lonsdale, Nonuniform magnetization of Jasper Seamount, *J. Geophys. Res., 93*, 12,159-12,175, 1988.

Gee, J., H. Staudigel, L. Tauxe, T. Pick, and Y. Gallet, Magnetization of the La Palma Seamount Series: Implications for seamount paleopoles, *J. Geophys. Res., 98,* 11, 743-11,767, 1993.

Guillou, H., M. Garcia, and L. Turpin, Unspiked K-Ar dating of young volcanic rocks from Loihi and Pitcairn hot spot seamounts, *J. Volcanol. Geotherm. Res., 78,* 239-249, 1997.

Harrison, C. G., A seamount with a nonmagnetic top, *Geophysics, 36*, 349-357, 1971.

Hildenbrand, T. G., J. Tosenbaum, and J. Kauahikaua, Aeromagnetic study of the island of Hawaii, *J. Geophys. Res., 98,* 4099-4119, 1993.

Holcomb, R. T. and R. C. Searle, Large landslides from oceanic volcanoes, *Mar. Geotech., 10*, 19-32, 1991.

Irving, E., The Mid-Atlantic Ridge at 45ºN. Oxidation and magnetic properties of basalt; Review and discussion, *Can. J. Earth Sci., 7*, 1528-1538, 1970.

Jensen, D. C. and J. C. Cain, An interim geomagnetic field, *J. Geophys. Res*., 67, 3568, 1962.

Johnson, H. P., and T. Atwater, Magnetic study of basalts from the Mid-Atlantic Ridge, lat 37°N, *Geol. Soc. Am. Bull., 88,* 637-647, 1978.

Johnson, H. P., and D. Clague, Magnetic properties of submarine basalt as a function of rock geochemistry: Samples from Loihi Seamount, Hawaii, *EOS Trans. AGU, 62,* 1082, 1981.

Johnson, H. P., J. L. Karsten, F. J. Vine, G. C. Smith, and G. Schonharting, A low-level magnetic survey over a massive sulfide ore body in the Troodos ophiolite complex, Cyprus, *Mar. Technol. Soc. J.,* 16, 76-79, 1982.

Johnson, H. P., and M. Tivey, Magnetic properties of zero-aged oceanic crust; a new submarine lava flow on the Juan de Fuca ridge, *Geophys. Res. Lett., 22*, 175-178, 1995.

Johnson, H. P., D. Van Patten, and W. Sager, Age-dependent variation in the magnetization of seamounts*, J. Geophys. Res., 101,* 13,701-13,714, 1996.

Karl, D. M., G. McMurtry, A. Malahoff, and M. Garcia, Loihi Seamount, Hawaii: A mid-plate volcano with a distinct hydrothermal system, *Nature, 335*, 532-535, 1988.

Keller, R. A., R. Duncan, and M. Fisk, Geochemistry and $^{40}AR/^{39}AR$ geochronology of basalts from ODP Leg 145 (North Pacific Transect), Proceedings of the Ocean Drilling Program, Scientific Results, 145, 333-344, 1995.

Klein, F. W., Earthquakes at Loihi submarine volcano and the Hawaiian hot spot, *J. Geophys. Res., 87*, 7719-7726, 1982.

Lenat, J., Structure et dynanique internes d'un volcan basaltique interplaque oceanique-le piton de la fournaise, Ph.D. thesis, 320 pp. series E, n. 394, L'Universite Blaise Pascal Clermont II, 1987.

Lenat, J., B. and Gibert-Malengreau, A new model for the evolution of the volcanic island of Reunion (Indian Ocean), *J. Geophys. Res., 106*, 8645-8663, 2001.

Loihi Science Team, Researchers rapidly respond to submarine activity at Loihi Volcano, Hawaii, *EOS Trans. AGU, 78*, 229-232, 1997.

Lonsdale, P., J. Dieu, and J. Natland, Posterosional volcanism in the Cretaceous part of the Hawaiian Hotspot Trail, *J. Geophys. Res., 98*, 4081-4098, 1993.

Malahoff, A., Geology of the summit of Loihi submarine volcano, in volcanism in Hawaii, *U.S. Geol. Surv. Prof. Pap., 1350,* 133-144, 1987.

Malahoff, A., G. McMurtry, J. Wiltshire, and H. Yeh, Geology and chemistry of hydrothermal deposit from active submarine volcano Loihi, Hawaii, *Nature, 298,* 234-239, 1982.

Malahoff, A. and G. P. Woollard, Magnetic surveys over the Hawaiian Islands and their geological implications, *Pac. Sci., 20*, 265-311, 1966.

Malahoff, A. and G. P. Woollard, Magnetic and tectonic trends over the Hawaiian Ridge, in *The Crust and Upper Mantle of the Pacific Area, Geophysical Monograph Series,* edited by L. Knopoff, C. L. Drake, and P. J. Hart, vol. 12, pp 241-276, AGU, Washington, D.C., 1968.

McNutt, M., Nonuniform magnetization of seamounts: A least squares approach, *J. Geophys. Res., 91,* 3686-3700, 1986.

Moore, J. G., D. A. Clague, and W. R. Normark, Diverse basalt types from Loihi Seamount, Hawaii, *Geology, 10,* 88-92, 1982.

Moore, J. G., W. R. Normark, and R.T. Holcomb, Giant Hawaiian landslides, *Ann. Rev. Earth Planet. Sci., 22,* 119-144, 1994.

Parker, R. and S. Huestis., The inversion of magnetic anomalies in the presence of topography, *J. Geophys. Res., 79*, 1587-1593, 1974.

Parker, R. L., L. Shure, and J. Hildebrand, The application of inverse theory to seamount magnetism, *Rev. Geophys., 25,* 17-40, 1987.

Plouff, D., Gravity and magnetic fields of polygonal prisms and application to magnetic terrain corrections, *Geophysics, 41,* 727-741, 1976.

Richards, M. L., V. Vacquier, and G. D. Van Voorhis, Calculation of the magnetization of uplifts from combining topographic and magnetic surveys, *Geophysics, 32,* 678-707, 1967.

Sager, W., Paleomagnetism of Abbott Seamount and implications for the latitudinal drift of the Hawaiian hot spot, *J. Geophys. Res., 89,* 1984.

Sager, W., Seamount age estimates from paleomagnetism and their implications for the history of volcanism on the Pacific plate, geology and offshore mineral resources of the central Pacific basin, *Circum-Pacific Council for Energy and Mineral Resources Earth Science Series*, 14, 21-37, 1992.

Sager, W., and M. Pringle, Paleomagnetic constraints on the origin and evolution of the musicians and south Hawaiian seamounts, Central Pacific Ocean, U.S. Geological Survey, Geophysical Monograph #43, 1987.

Staudigel, H., A. Zindler, S. R. Hart, T. Leslie, C.-Y. Chen, and D. Clague, The isotope systematics of a juvenile intraplate volcano: Pb, Nd, and Sr isotope ratios of basalts from Loihi Seamount, Hawaii, *Earth Planet. Sci. Lett., 69,* 13-29, 1984.

Stewart, R., and J. Joy, HF radio measurements in surface currents, *Deep Sea Res. Ocean. Abs., 21,* 1039-1049, 1974.

Takagi, M., A. Iwata, and K. Masai, A possible effect of atmospheric and terrestrial physics, *J. Atmos. Terr. Phys*., 42, 683-686, 1980.

Talwani, M., Computation with the help of a digital computer of magnetic anomalies caused by bodies of Arbitrary Shape, *Geophysics, 30,* 797-817, 1965.

Tivey, M., Fine-scale magnetic anomaly field over the southern Juan de Fuca Ridge: Axial magnetization low and implications for crustal structure, *J. Geophys. Res., 99,* 4833-4855, 1994.

Tivey, M., and P. Johnson, The magnetic structure of Axial Seamount, Juan de Fuca Ridge, *J. Geophys. Res., 95,* 1990.

Walker, G., Volcanic rift zones and their intrusion swarms, *J. Volcanol. Geotherm. Res., 94,* 21-34, 1999.

Watkins, N., and T. Paster, The magnetic properties of igneous rocks from the ocean floor, *Philos. Trans. R. Soc. London A., 268,* 507-550, 1971.

Wessel, P., XOVER: A cross-over error detector for track data, *Comp. Geosciences, 15*, 333-346, 1989.

Wessel, P. and W. Smith, Free software helps map and display data, *EOS Trans. AGU, 72*, 445-446, 1991.

VITA

Amy J. Lamarche

Personal Information
Address: 87 Pleasant Terr. Leominster, MA 01453
Phone: (978) 534-3865
e-mail: aj@ocean.tamu.edu

Education B.S. December, 1999, Earth Science, Fitchburg State College, Fitchburg, MA

Research Experience

1/01-8/03 Research Assistant in Geophysics/Oceanography, Department of Oceanography, Texas A&M University.
Supervisor/Chair of Committee: Dr. William Sager
Responsibilities: Modeled the magnetic field of submarine volcanoes, analysis of Alternating Field Demagnetization (AFD), and susceptibility measurements of submarine volcanic samples.

Cruise Experience

11/02-1/03 Investigated the Magnetic Jurassic Quiet Zone using a magnetometer towed 90 m off the seafloor in the North Pacific Ocean. Data was collected aboard the R/V *Thomas Thompson*.

4/28-5/1/03 Research cruise imaging Sabine Bank, Gulf of Mexico using side-scan sonar. Data was collected aboard the R/V *Marie Hall*.

Teaching Experience

10/12/02 Speaker, Expanding Your Horizons, Texas A&M University.
Responsibilities: Generated and presented a module to initiate an interest in science to 6th grade girls.

9/01-12/01 Teaching Assistant, Department of Oceanography, Texas A&M University.
Responsibilities: Lead 2 lab sections once per week, including lecturing, grading, and demonstrating experiments for Introductory Oceanography.

Professional Development Conferences

5/01 & 5/03 Offshore Technology Conference (OTC), Houston,TX

Organization Memberships

9/01-12/03 Oceanography Graduate Council (OGC), Texas A&M University.
Offices Held: Geological section representative and Treasurer.

4/04-present American Geophysical Union.

Awards

1999 Department of Geophysics Student of the Year, Fitchburg State College.

2003 Student Research Week, poster session 1st place, Texas A&M University.